



# Modeling the westward transversal current in the southern Yellow Sea entrance: a case study in winter 2007

Yang Ding<sup>1</sup> · Xianwen Bao<sup>1,2</sup> · Lingling Zhou<sup>2</sup> · Congcong Bi<sup>2</sup> · Zhigang Yao<sup>1,2</sup> · Chao Ma<sup>1,2</sup> · Qinqin Chu<sup>3</sup>

Received: 7 October 2019 / Accepted: 16 March 2020 / Published online: 3 April 2020  
© Springer-Verlag GmbH Germany, part of Springer Nature 2020

## Abstract

The westward transversal current (TC) in the southern Yellow Sea entrance was investigated during winter 2007 using a numerical ocean model. The three-dimensional structures and dynamics of the westward TC were highlighted. The model-simulated monthly mean current fields showed that the strong westward TC was limited to the upper water column (shallower than 50 m) and extended westward from 126° E to 124° E. Momentum balance analysis indicated that the westward TC was mainly regulated by a quasi-geostrophic balance. Both the sea surface elevation-related barotropic pressure gradient force and the density-related baroclinic pressure gradient force controlled the intensity and direction of the westward TC. Sensitivity model experiments focusing on tide and wind demonstrated that the westward TC was intensified when tide was ignored and was greatly weakened when wind was excluded. Lagrangian particle tracking experiments were also performed, to investigate the relationship between the Yellow Sea Warm Current and the westward TC in the frontal region. The characteristics of the water in the Yellow Sea Warm Current were affected by the properties of the water in the frontal zone, especially in the sub-surface and lower layers. The westward TC might act as an important bridge, connecting the frontal zone with the Yellow Sea Warm Current flowing along the western Yellow Sea trough.

**Keywords** Southern Yellow Sea · Thermohaline front · Frontal circulation · Westward transversal current · Yellow Sea Warm Current · Modeling study

---

This article is part of the Topical Collection on the *11th International Workshop on Modeling the Ocean (IWMO), Wuxi, China, 17–20 June 2019*

---

Responsible Editor: Zhiyu Liu

---

**Electronic supplementary material** The online version of this article (<https://doi.org/10.1007/s10236-020-01361-9>) contains supplementary material, which is available to authorized users.

---

✉ Zhigang Yao  
yaozhigang@ouc.edu.cn

- <sup>1</sup> Key Laboratory of Physical Oceanography/Institute for Advanced Ocean Studies, Ocean University of China and Qingdao National Laboratory for Marine Science and Technology, Qingdao, China
- <sup>2</sup> College of Oceanic and Atmospheric Sciences, Ocean University of China, Qingdao, China
- <sup>3</sup> QHD Marine Environmental Central Station of SOA, Qinhuangdao, Hebei, China

## 1 Introduction

In the winter, both remote sensing and in situ hydrographic data show a thermohaline front originating from Jeju-do and invading the Yellow Sea (Asaoka and Moriyasu 1966; Nakao 1977; Lie 1984; Park and Chu 2006; Huang et al. 2010; Lin et al. 2011; Lin and Yang 2011). The edges of this giant tongue form sharp fronts where the warm Kuroshio saltwater meets the cold costal freshwater (Lie et al. 2013, 2015; Lie and Cho 2016). The front extension of the tongue is usually inclined to the north with increasing depth, forming a wedge-shaped structure (Lie et al. 2013). This wedge-shaped front causes frequent occurrences of temperature inversion within the frontal zone (Kim et al. 1982; Hao et al. 2010; Lie et al. 2013, 2015; Pang et al. 2017). The northern front of the tongue usually runs westward along 34° N, across the deep trough of the southern Yellow Sea (Lie 1985); cold freshwater from the southward Korea Coastal Current is found north of the northern front, while warm saltwater from the Cheju Warm Current is found south of the northern front (Lie et al. 2009). To the south, the cold freshwater from the Chinese coast

generally follows the southern front, flowing along the 50-m isobaths in Changjiang Bank (Lie and Cho 2016). The thermohaline front in the southern Yellow Sea is fundamentally dynamic and thus holds a very prominent position, affecting both regional circulation and the interactions between the Yellow Sea and the East China Sea (Lie et al. 2009). The hydrographic distribution associated with the frontal structure also significantly affects thermohaline momentum, as well as the rate of nutrient transport into the Yellow Sea interior (Guan 1962; Su et al. 2005; Lin et al. 2011; Jin et al. 2013; Liu et al. 2015).

The circulation of the southern Yellow Sea during the winter has been well investigated (Lie et al. 2013, 2015; Lie and Cho 2016). Previous observational and modeling studies in the southern Yellow Sea identified two downwind coastal currents that bring cold freshwater southward: the Chinese Coastal Current and the Korea Coastal Current (Lie 1984; Guan 1994; Ichikawa and Beardsley 2002; Yuan et al. 2008; Lie et al. 2013; Lie and Cho 2016). In opposition, the Cheju Warm Current, carrying warm saltwater from the Kuroshio system, flows northwestward around Jeju-do, south of the northern front (Lie et al. 2013). Northwestward intrusions of the Cheju Warm Current are occasionally observed, indicating an upwind flow along the west flank of the Yellow Sea trough (Lie et al. 2001, 2009); this flow is known as the Yellow Sea Warm Current (Lie et al. 2001). The Yellow Sea Warm Current is a striking winter phenomenon that exerts a strong, dynamic, thermal influence on the Yellow Sea and the Bohai Sea (Lie et al. 2001; Bao et al. 2004; Isobe 2008; Wei et al. 2010; Liu et al. 2015).

Although previous studies have reported detailed patterns of regional circulation in the southern Yellow Sea, knowledge of the current system in the frontal zone remains limited. This is because circulation in the frontal region during the winter is rather complicated, and observational data are extremely rare due to intensive fishing activity (Lie et al. 2013, 2015). Based on in situ data (conductivity-temperature-depth (CTD), float trajectories, currents, and wind), Lie et al. (2013) proposed regional circulation pattern in the frontal zone, emphasizing that the cold water from the southward Korea Coastal Current moves westward along the northern front before turning cyclonic around the warm tongue to run southeastward along the southern front. Lie et al. (2013), relying on geostrophically calculated currents and float trajectories, proposed a westward transversal current (TC) flow, approximately along  $34^\circ$  N, and a cold-water cyclonic front. The TC mixed with both cold freshwater from the Korean coastal region and warm saline water from Cheju Warm Current may have a crucial effect on the regional circulation in this area.

The Yellow Sea Warm Current, originating from the warm saline tongue (Lie et al. 2001), might be significantly influenced by frontal circulation, as well as by the TC and other currents. However, our understanding of frontal circulation, as

well as its impact on the Yellow Sea Warm Current, remains limited, partly due to the lack of observations. In addition, previous numerical models of the frontal structure and the TC were not well resolved. The impact of the westward TC on the Yellow Sea Warm Current still requires clarification. To date, the most valuable observational study of the westward TC comes from Lie et al. (2013), who provided evidence of the westward TC via both geostrophically calculated currents and float trajectories. Unfortunately, Lie et al. (2013) could not characterize the structure of the westward TC in detail due to observational limits.

Numerical ocean models are powerful tools with which to investigate the characteristics and mechanisms of frontal circulation. To our knowledge, one numerical model of the westward TC is available, which is focused on the formation and structure of the westward TC using a two-dimensional vertical slice model (Oh et al. 2015). However, a more accurate and reliable three-dimensional simulation based on realistic bathymetric and surface atmospheric forcing data would more fully allow a diagnostic examination of frontal dynamics and circulation, especially those of the westward TC.

Here, we first describe and validate our ocean model (Sect. 2). We then quantify the features of frontal circulation and the westward TC (Sect. 3) and use sensitivity experiments to investigate the effects of tide and wind on frontal circulation and the westward TC (Sect. 4). Next, we analyze the impact of the westward TC on the Yellow Sea Warm Current (Sect. 5). Finally, we discuss and summarize our results (Sect. 6).

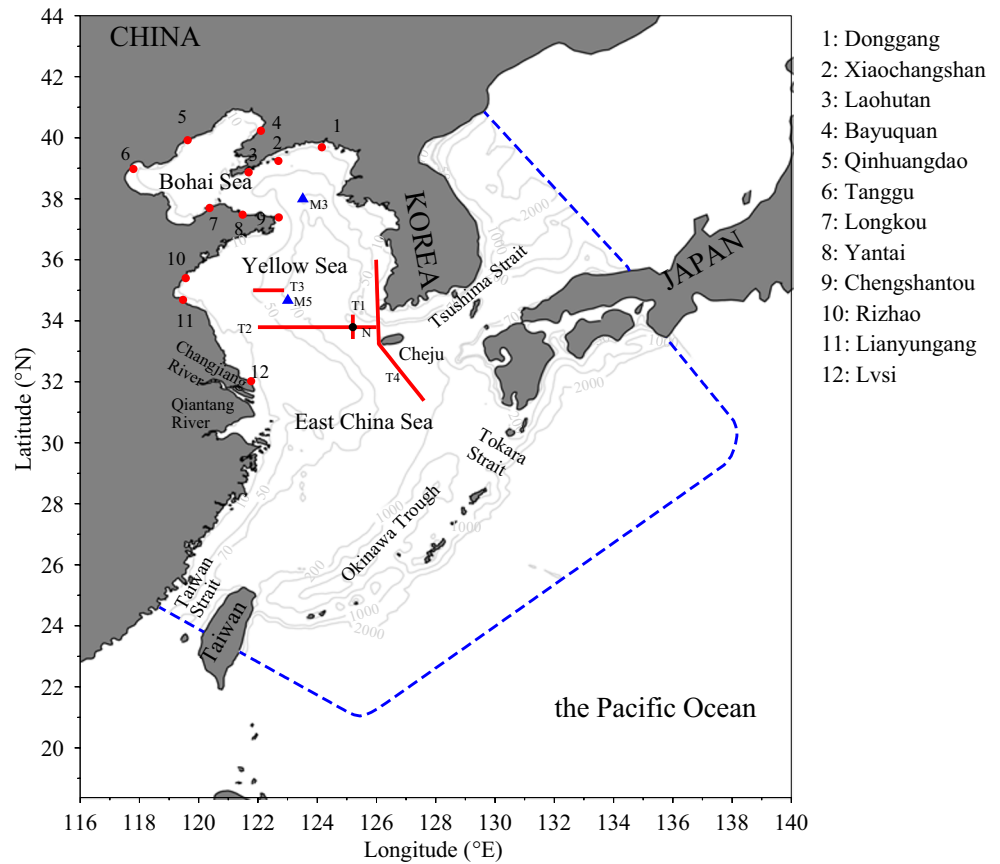
## 2 Model description and model validation

### 2.1 Ocean model

In this study, we adopted the unstructured-grid Finite Volume Community Ocean Model (FVCOM, Chen et al. 2003; Chen et al. 2007), as this model has been frequently and successfully used in previous multi-scale studies of ocean processes in the Yellow Sea and the East China Sea (Chen et al. 2008; Xue et al. 2009; Ding et al. 2011; Ge et al. 2015; Xuan et al. 2017).

Our model domain covered the Bohai Sea, the Yellow Sea, and the East China Sea, extending from  $21^\circ$  N to  $41^\circ$  N and from  $117^\circ$  E to  $138^\circ$  E (Fig. 1). Spatially, the horizontal resolution varied from 1 km along the coasts of the Bohai Sea and the Yellow Sea to 20 km at the open boundaries (blue dashed line in Fig. 1), with 30 vertical layers of terrain-following coordinates. The bathymetric data were obtained from DBDB5 (US Naval Oceanographic Office 1983) and were optimized in coastal area using marine navigational charts. Surface-forcing data, consisting of sea-level pressure, sea surface wind, long-wave radiation, short-wave radiation, air temperature, relative humidity, precipitation, and evaporation, were derived from the hourly dataset of the Climate Forecast

**Fig. 1** Map of the studied region and model domain including the Bohai Sea, Yellow Sea, and East China Sea. The gray lines denote the isobaths. Blue dashed lines denote the open boundaries of the region model. The current mooring stations (M3 and M5) are marked by blue triangles. Red dots denote the coastal sea-level stations. The meridional transect T1 and zonal transect T2 (red lines) in the frontal region are selected to show the vertical structure of the westward transversal current. A zonal transect (T3) extending from the 50- to 70-m isobath across the pathway of the Yellow Sea Warm Current (YSWC) is selected, and the volume transport is estimated. Transect T4 is chosen to evaluate the effect of Korea Coastal Current and Cheju Warm Current on the TC. The black dot (N) in the frontal region denotes a station where the currents, temperature, and salinity are sampled



System Reanalysis (CFSR) of National Center for Environmental Prediction (NCEP, <https://rda.ucar.edu/datasets/ds093.1/>). The surface latent and sensible heat flux are calculated based on bulk formulation (Fairall et al. 1996). No thermal correction to the heat flux was used in the model simulations. Sea surface height, velocity, temperature, and salinity were extracted daily from HYCOM (Hybrid Coordinate Ocean Model, Bleck 2002; Chassignet et al. 2007), to provide the initial conditions and the open boundary conditions. The variables from HYCOM were interpolated onto the unstructured FVCOM grids. Tidal effects (i.e.,  $M_2$ ,  $S_2$ ,  $N_2$ ,  $K_1$ ,  $O_1$ ,  $Q_1$ ,  $M_4$ ,  $MS_4$ ,  $MN_4$ ) were obtained from TPXO 7.2 (Egbert and Erofeeva 2002), in order to account for tidal forcing on sea surface elevations and barotropic currents along the open boundaries. Discharges from two major rivers (the Changjiang and the Yellow River) were also included in the model as mean monthly runoff volumes, provided by the Bureau of Hydrology, Ministry of Water Resources, P. R. China. Our model was previously used to investigate the synoptic variations of the Yellow Sea Warm Current (Ding et al. 2018).

In winter 2007, a mooring was deployed in the southern Yellow Sea, close to the frontal region, by the First Institution of Oceanography, State Oceanic Administration, (Fig. 1, M5). Observations were made for more than 30 days, during which

time 12 additional coastal tide gauges along the Chinese coast measured the sea level (Fig. 1). These long-term direct current observations provided valuable insight into the Yellow Sea Warm Current, even though the mooring was not directly inside the frontal zone. In this paper, we mainly focused on winter 2007. The simulation ran from January 1, 2005, until December 31, 2007. The hourly outputs from January to February 2007 were used for the following analyses.

## 2.2 Model validation

### 2.2.1 Sea level elevation

Sea level was investigated first (Fig. 2), after removing the tidal signal using a 40-h low-pass filter (Beardsley and Rosenfeld 1983). Sub-tidal variations in sea level were well reproduced by our model at all 12 stations, as evidenced by the strong correlation between the simulated time series and the observed time series. Our model successfully reproduced the dramatically sharp drop in sea level (January 6–9 and February 14–17), which might have been caused by winter storm outbreaks. It should be noted that our model overestimated the sea level during two periods: January 20–30 and February 10–25. In addition, a phase shift was also identified between the model and the

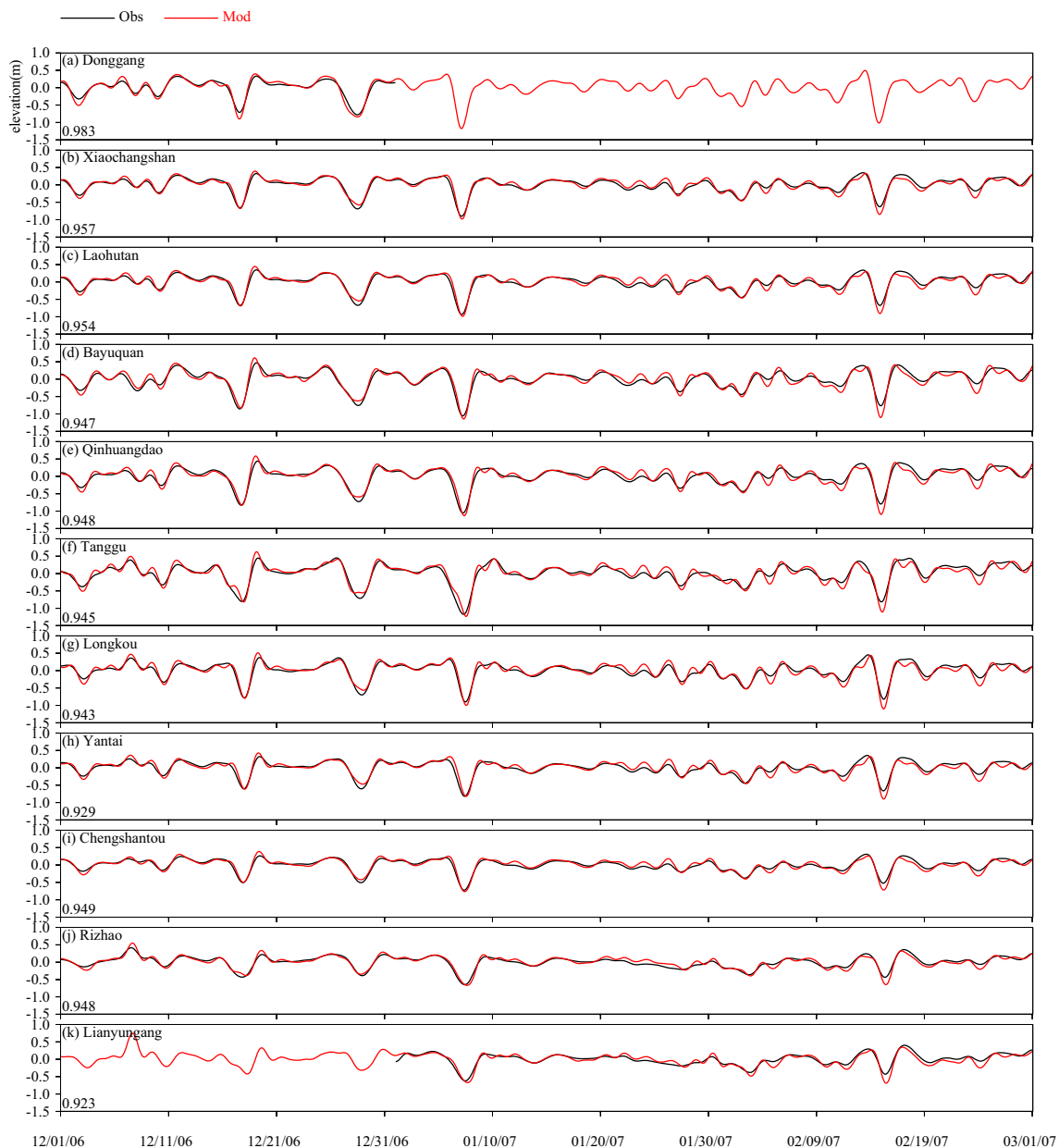


**Fig. 2** Comparison of sub-tidal sea level elevations at the 12 coastal stations during winter 2007 between model results (red) and the observations (black). The correlation coefficients between the model-simulated

and observed sea level time series are also embedded in the figure. This comparison of sea level elevation can also be found in Ding et al. (2018)

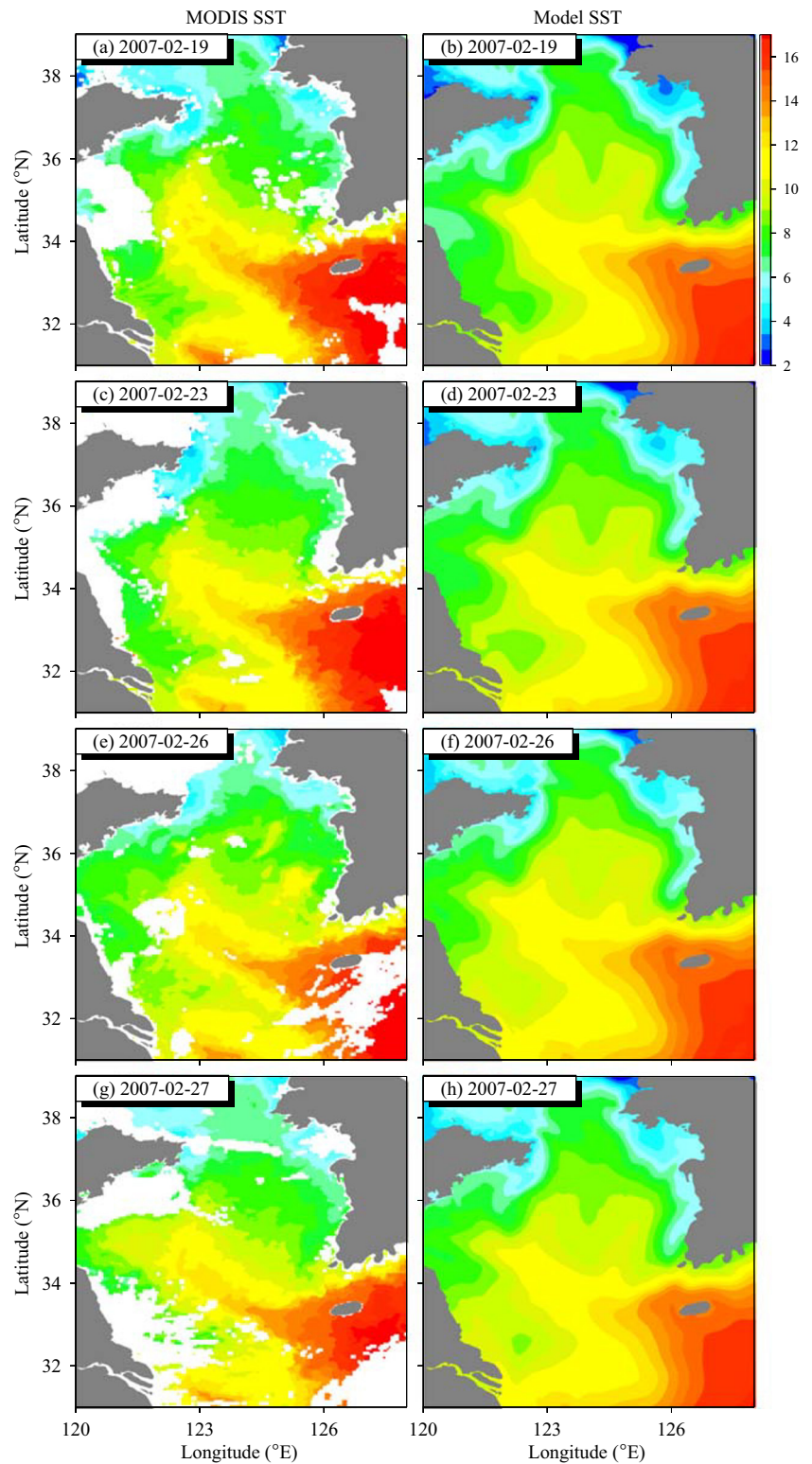
observations at Lvsi, which might have arisen due to the coarse resolution and bathymetric errors that are common in complex coastal area.

### 2.2.2 SST

Sea surface temperature (SST) is a key variable in frontal studies. The daily SST in the region model was compared with the satellite-derived SST from Moderate Resolution Imaging Spectroradiometer (MODIS-Aqua) with spatial resolution of 4 km. The monthly mean SST in the region model was also compared with the MODIS data and shown in Fig. S1 in the

Supplementary Material. As the SST data from MODIS in the Yellow Sea are often missed at daily interval, we only obtained several days when the daily SST data cover nearly the whole Yellow Sea. Thus, we selected days 19, 23, 26, and 27 in February to compare with the model results (Fig. 3). It can be seen that the spatial patterns of the SST were similar between the model and the observations, especially the warm tongue and the thermal fronts. The water temperature is relatively high in the region southeast of Jeju-do and is lower in the shallower Yellow Sea. The most important feature in this region is the warm tongue with temperature higher than 12 °C extending northwestward into the Yellow Sea (YS) interior,

**Fig. 3** Comparison of daily sea surface temperature between Moderate Resolution Imaging Spectroradiometer (MODIS) data (left panel) and the model (right panel) on February 19, 23, 26, and 27



which can be noted in both the satellite data and model results. Sharp fronts appeared when the cold coastal water met the warm water from the Kuroshio; the Kuroshio water occupied a vast region south of Jeju-do and formed the giant warm tongue. A cold tongue extending southeastward from China

coast can also be noted in both the observations and simulations. The sharp front north and southwest of Jeju-do was also reproduced by the model. A separation of the warm tongue toward the Korea coast can often be seen, such as on February 23 and 26. This branch of the warm tongue was captured by

the model but was often overestimated, such as on days 19 and 27 of February. The warm tongue in the model sometimes extended further northward compared with the satellite data (February 19 and 26). The discrepancy between the satellite data and model might be mainly due to the inaccuracy of the surface-forcing data (including wind and heat flux) used in the model. It should also be noted that the model that simulated the spatial pattern of the SST was too smoothed compared with that from the MODIS data. This may be caused by the too strong diffusion in the model setup. The horizontal diffusion coefficient was set to be 0.2 in the current model simulations, which seemed to be too large for the southern Yellow Sea region. Besides, the horizontal resolution of the model mesh may be not high enough to resolve the finer structures of the SST in the YS.

### 2.2.3 Sub-tidal currents and circulation pattern around the frontal zone

Modeled and observed sub-tidal currents at mooring station M3 were compared (Fig. 4a). We found that the model generally captured the low-frequency variations in the currents at M3 (Fig. 4a). Both the observations and the model simulations identified significant synoptic variations in the current at the mooring station. It should be noted that the simulated current was more barotropic with less vertical shear compared with the observations. The station M3 is located in the end of the

Yellow Sea Warm Current, and the current at this station is featured with strong synoptic variability. The model results are often not good especially when the observed current is too weak. However, the episodic northwestward current bursts during multiple winter storm bursts can generally be resolved by the model. For example, current fluctuations during the storm event (January 6–9) were accurately captured by the model. There were some discrepancies in current magnitude and direction between the model-simulated time series and observed time series, which may be mainly caused by the inaccurate surface wind forcing and bathymetry. Moreover, the vertical resolution of the model may also influence the simulated results. Although we did not obtain data from mooring station M5 (deployed by the First Institution of Oceanography, State Oceanic Administration at 73-m depth in the western Yellow Sea at about 34.67° N; Yu et al. 2010), we did check the figure of observed low-passed currents in January 2007 (Fig. 7 in Yu et al. 2010). A strong, stable northwestward Yellow Sea Warm Current was identified during January 5–22 in both the observed data (Fig. 7 in Yu et al. 2010) and our model results (Fig. 4b).

Current simulations were also validated by comparing the circulation pattern with that projected based on in situ CTD data and float trajectories (Fig. 5; Lie et al. 2013; Lie and Cho 2016). The Tsushima Warm Current and the Cheju Warm Current from Kuroshio were reasonably resolved (Fig. 5b). Additional circulation patterns were also well modeled,

**Fig. 4** Comparison of sub-tidal currents at mooring station M3 (a) during winter 2007 between the model simulations (red) and the observations (black). The model-simulated sub-tidal currents at station M5 is shown in b. The observed sub-tidal current at station M5 can be found in Fig. 7 of Yu et al. (2010)

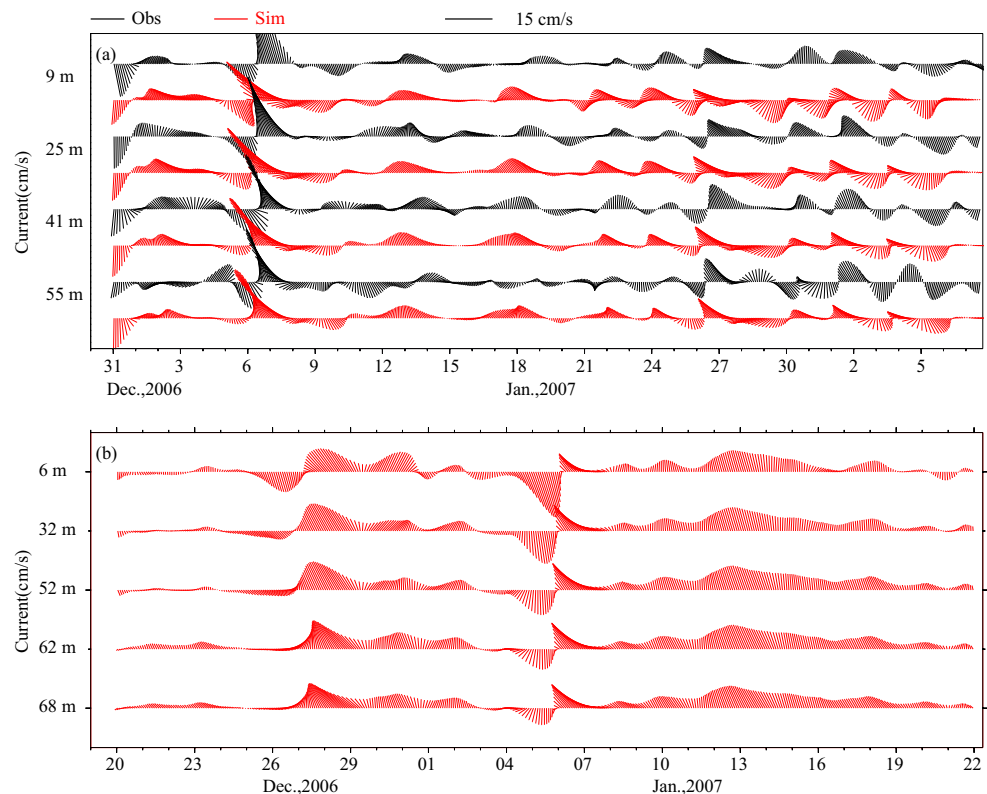
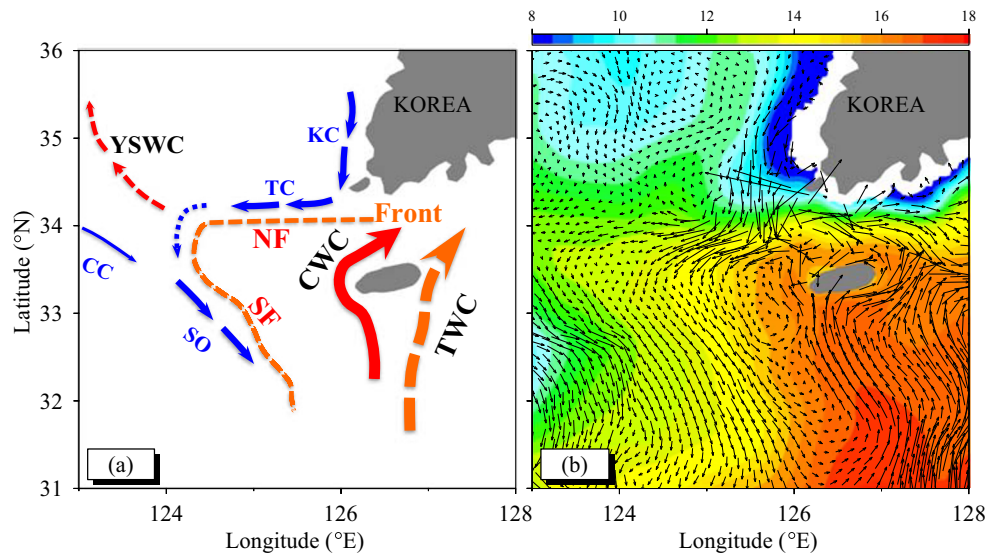


**Fig. 5** Comparison of circulation pattern at 10-m depth during winter between the observations (a) and model (b). The observed circulation pattern is redrawn from Lie et al. (2013) and Lie and Cho (2016). TWC Tsushima Warm Current, CWC Cheju Warm Current, KC Korea Coastal Current, TC Transversal Current, YSWC Yellow Sea Warm Current, CC Chinese Coastal Current, SO Southeastward Outflow, NF northern front, SF southern front



including the southward Korea Coastal Current along the Korean coast, the westward TC along the northern warm tongue, the cyclonic turning of the TC at the tip of the warm tongue, and the merging of the TC with the southeastward outflow from the Chinese Coastal Current along the 50-m isobath; these patterns were consistent with previous findings (Lie et al. 2013; Lie and Cho 2016).

It should be noted that the intensity of model-simulated Cheju Warm Current was relatively weaker compared with the observations as also mentioned by one of the reviewers. The simulated monthly mean current in January and February 2007 focusing on the Cheju Warm Current is shown in Fig. S2 in the Supplementary Material. The Cheju Warm Current was very weak in the monthly mean field of February (Fig. S2b, d, f). Although the monthly mean Cheju Warm Current in January was not strong enough, the anti-cyclonic turn of the Cheju Warm Current was generally resolved. From the monthly mean wind from CFSR in January and February 2007, we can note that the northwesterly wind was greatly decreased in the Yellow Sea in February (Fig. S3b). We also checked the simulation results in the winter of year 2017 (Fig. S4). The cyclonic Cheju Warm Current was obvious in both January and February 2017, especially in lower layers (30-m and 50-m depth). Wind forcing indicated that both January and February of year 2017 featured strong northwesterly wind in the Yellow Sea. Therefore, the simulated intensity of the Cheju Warm Current may be closely related to the wind forcing in winter.

The mean current averaged over January 1–5, January 6–10, and January 11–15 is shown in Fig. S5 in the Supplementary Material. It is interesting to note that pattern of the Cheju Warm Current was quite different for the three periods during January. The water generally moved eastward south of Jeju-do, and the Cheju Warm Current was not present during January 1–5 (Fig. S5a, d, g). There was significant northwestward intrusion southwest of Jeju-do for Cheju

Warm Current during the period of January 6–10 (Fig. S5b, e, h). The anti-cyclonic turn of the Cheju Warm Current around the Jeju-do was obvious during the time of January 11–15 (Fig. S5c, f, i). The surface wind field during the three periods also showed very different patterns (Fig. S6), which further tells us that the simulated pattern of the Cheju Warm Current may be highly affected by the surface wind. On the other hand, the variations of the Cheju Warm Current may be closely correlated with the Kuroshio. Therefore, variability of the Kuroshio may lead to changes of the intensity of the Cheju Warm Current. It should also be kept in mind that the inaccurate surface wind forcing and bathymetry around the Jeju-do area can affect the simulation of the Cheju Warm Current. Moreover, the uncertainty of the open boundary for the Kuroshio may also lead to discrepancy in simulating the Cheju Warm Current.

### 3 Model-simulated circulation in the frontal zone in winter 2007

#### 3.1 Formation and evolution of the front

The front in the southern Yellow Sea entrance is mainly responsible for driving the westward TC. Therefore, we first discuss the formation mechanism and evolution of the thermal front in the southern Yellow Sea entrance. It should be noted that the main processes determining the northern thermal front have been investigated by Wang et al. (2012). The cold water advected by the southward coastal current driven by northerly wind and the local cooling during the winter season control the mean meridional location of the northern thermal front in the southern Yellow Sea entrance. They also suggested that the intensity of the northern thermal front was

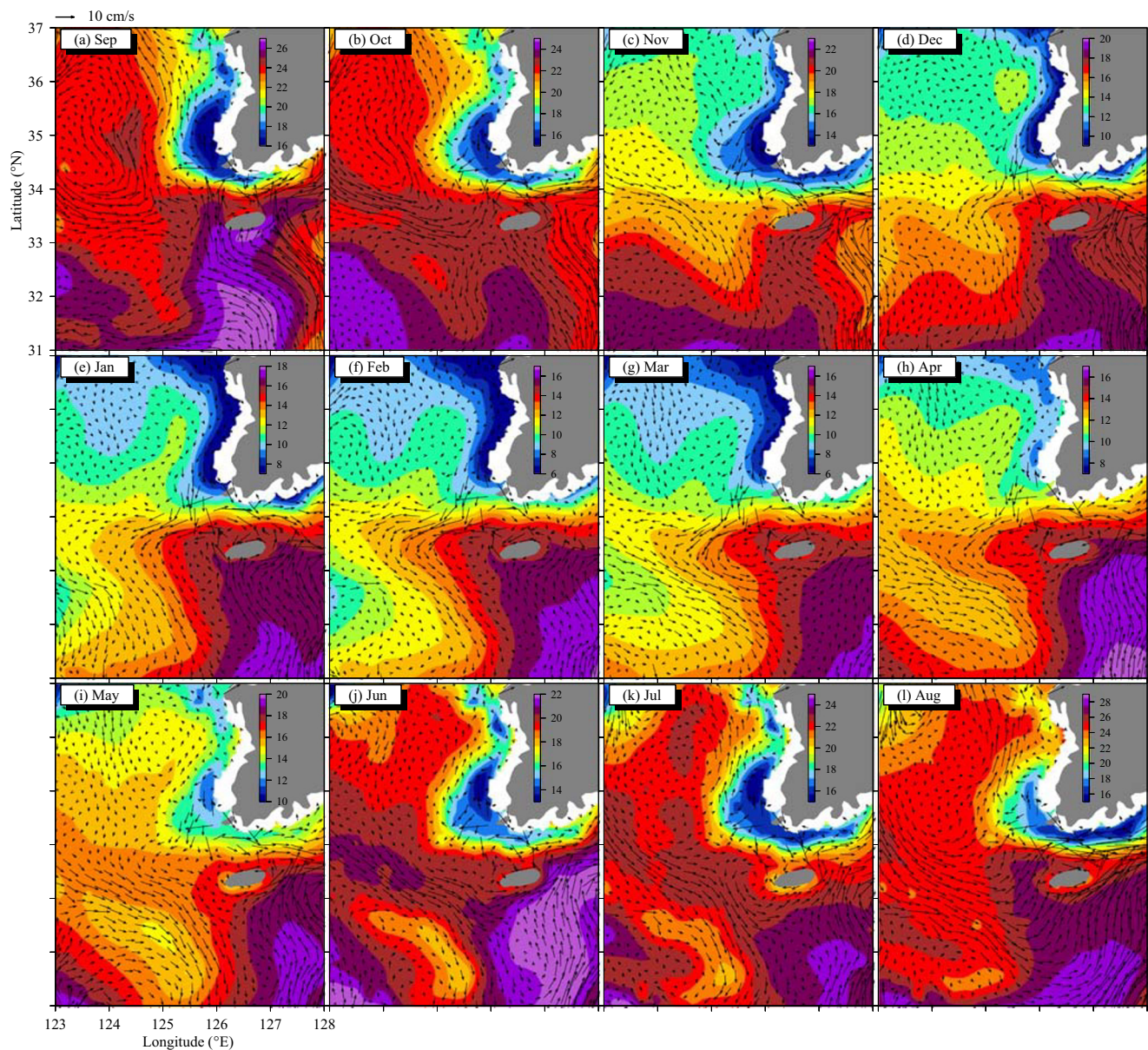


**Fig. 6** Model-simulated monthly mean current and temperature at 10-m depth in the frontal region from September 2006 to August 2007

related to the warm water originated from the Yellow Sea Warm Current south of the front.

Figure 6 shows the evolution of monthly mean surface current and temperature at 10 m from September 2006 to August 2007. In September and October (Fig. 6(a), (b)), there was no signal for the front as the temperatures were generally high exceeding 24 °C in most area of the southern Yellow Sea except the coastal region west of Korea. The thermal front began to form in November when the shallower southern Yellow Sea became colder. The front gradually strengthened from December to February and reached maximum intensity in February (Fig. 6(d)–(f)). The cyclonic frontal circulation also became robust in January and February (Fig. 6(e), (f)). The front and cyclonic frontal circulation still existed in early

spring of March and April with reduced intensity (Fig. 6(g), (h)). The front began to disappear in May as the water in the southern Yellow Sea became warmer and warmer. The frontal circulation also cannot be detected from late spring until late autumn. We can also note that the thermal front cannot occur in summer and early autumn months, when most regions of the southern Yellow Sea were characterized by higher water temperature (Fig. 6(j)–(l)).

To further illustrate the formation mechanism of the thermal front, a transect crossing the coastal region of Korea and also the region south of Jeju-do (T4 in Fig. 1) was chosen to show the meridional current velocity and temperature during different months (Figs. 7 and 8). We can note that the northward Tsushima Warm Current and Cheju Warm Current south



of the Jeju-do were present in each month during the whole year. However, the condition for the southward Korea Coastal Current was different. The southward Korea Coastal Current mainly occurred from November to March and was able to bring the cold freshwater southward to the frontal region. The temperature distribution along transect T4 showed that the water was more stratified during summer and early autumn months, which was not favorable for the formation of the thermal front. It can also be noted that the water was well mixed due to strong wind in winter. During winter the region north of Jeju-do lost much more heat than the southern region due to shallower water depth, which caused the temperature to be much lower in the north than that in the south. On the other hand, the southward Korea Coastal Current from November to March (Fig. 7(c)–(g)) was significant and advected the colder water southward (Fig. 8(c)–(g)), meeting the relatively warmer water from the Tsushima Warm Current and Cheju Warm Current and was essential for the formation of the front in the southern Yellow Sea entrance.

It can be concluded based on the above analysis that the nonuniform heat loss causes much lower temperature in the shallower coastal region north of Jeju-do, which is important for the meridional temperature gradient in the frontal region. On the other hand, the northward Tsushima Warm Current and Cheju Warm Current south of Jeju-do bring warmer water

northward and the Korea Coastal Current advects colder water southward, which is also crucial for the formation of the front in the southern Yellow Sea entrance.

### 3.2 Horizontal distribution of the frontal circulation

The monthly mean currents and temperatures at depths of 10 m, 30 m, 50 m, and 70 m in the southern Yellow Sea in January and February 2007 were simulated using the model (Fig. 9). The cyclonic circulation around the warm tongue was clear in the upper layer (Fig. 9(a)–(d)), but this circulation pattern was less obvious with increasing depth. At 10 m deep, cyclonic circulation around the warm tongue dominated, in contrast to the anti-cyclonic Cheju Warm Current around Jeju-do (Fig. 9(a), (b)). The currents flowed westward along the northern front, made a cyclonic turn around the western tip of the front, and continued to move southeastward along the southern front. This pattern was consistent with the results of previous studies (Lie et al. 2013; Lie and Cho 2016). In the lower layer, the cyclonic circulation around the warm tongue weakened noticeably (Fig. 9(e), (f)), and disappeared in the bottom layer (Fig. 9(g), (h)). In the bottom layer (70-m depth), the cyclonic circulation around the front was replaced by the northward Cheju Warm Current.

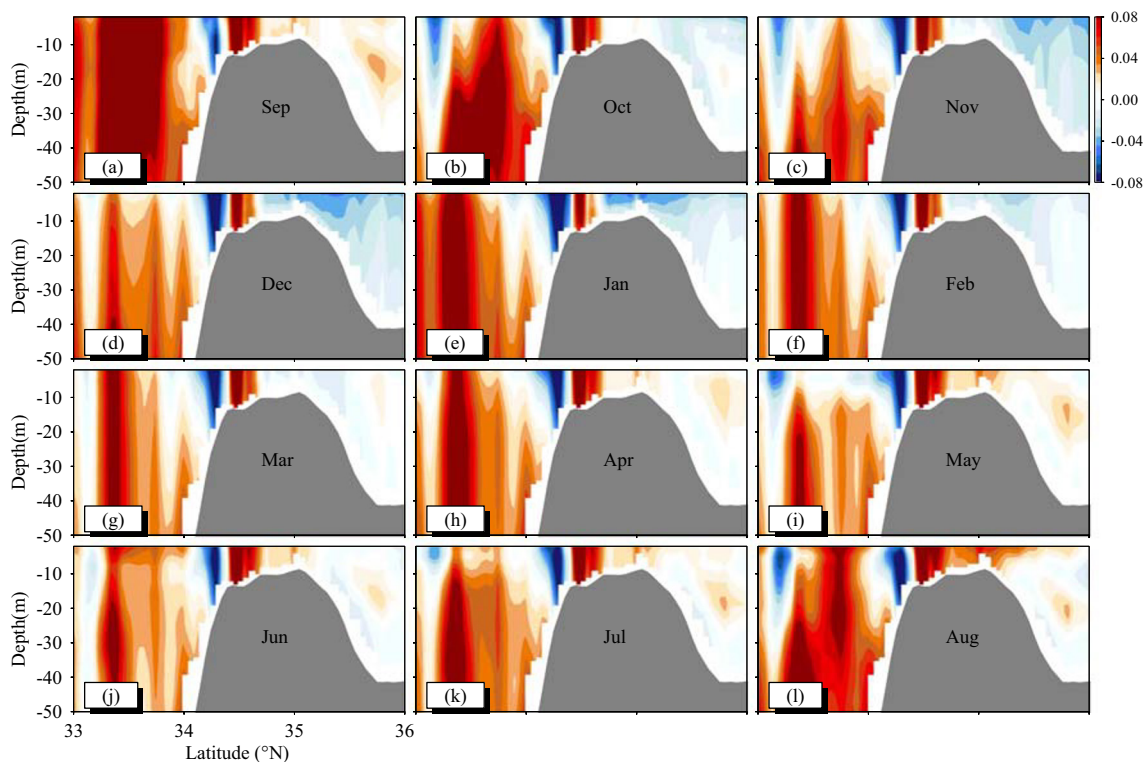


**Fig. 7** Model-simulated monthly mean meridional current component along section T4 from September 2006 to August 2007. The positive

value denotes northward current. The location of transect T4 is shown in Fig. 1

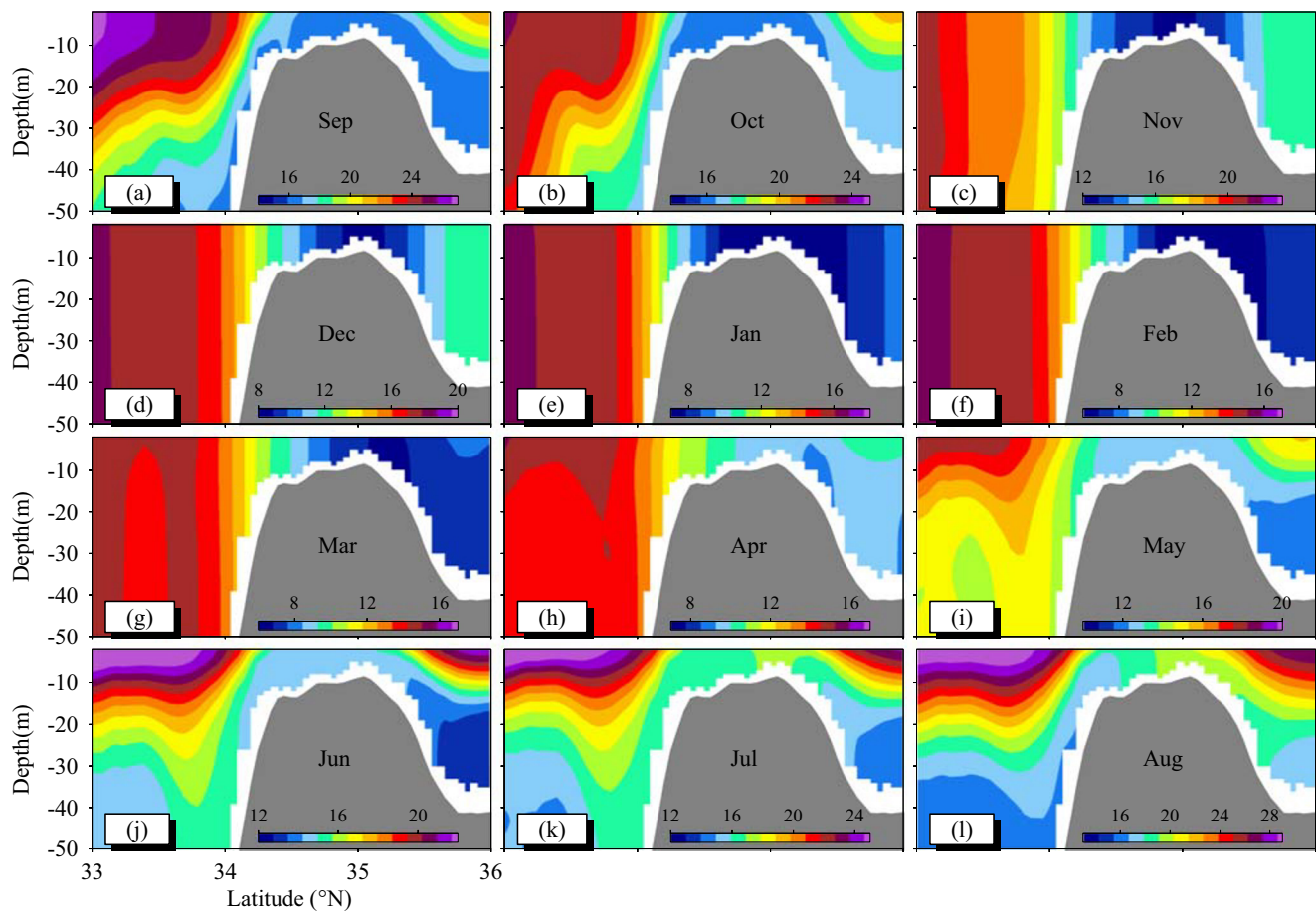


**Fig. 8** Model-simulated monthly mean temperature along section T4 from September 2006 to August 2007

The westward TC in the northern front zone was most remarkable at the surface, with maximum magnitude exceeding 15 cm/s. The velocity of the TC decreased gradually with depth, consistent with observations in this region (Lie et al. 2013; Oh et al. 2015). In the surface layer (10-m depth), the westward TC appeared to be a continuation of the southward Korea Coastal Current. However, in the sub-surface layer (30 m), both the cold, fresh, southward Korea Coastal Current from the north and the warm, saline, northwestward Cheju Warm Current from the south contributed to the westward TC. At 50-m depth, the westward TC was weaker, with a velocity of only 5 cm/s, and was closely related to the northwestward intrusion of the Cheju Warm Current. However, the westward TC was not observed at 70-m depth. Notably, the westward TC extended in the east-to-west direction from 126° E to 124° E. The horizontal scale of the TC is estimated to be 100–200 km in the east-west direction and 50–70 km in the north-south direction, which is much larger than the first baroclinic Rossby radius of deformation (Fig. S7 in the Supplementary Material). Part of the water from the westward TC was advected northwestward and joined the Yellow Sea Warm Current at 30-m depth. The westward TC was

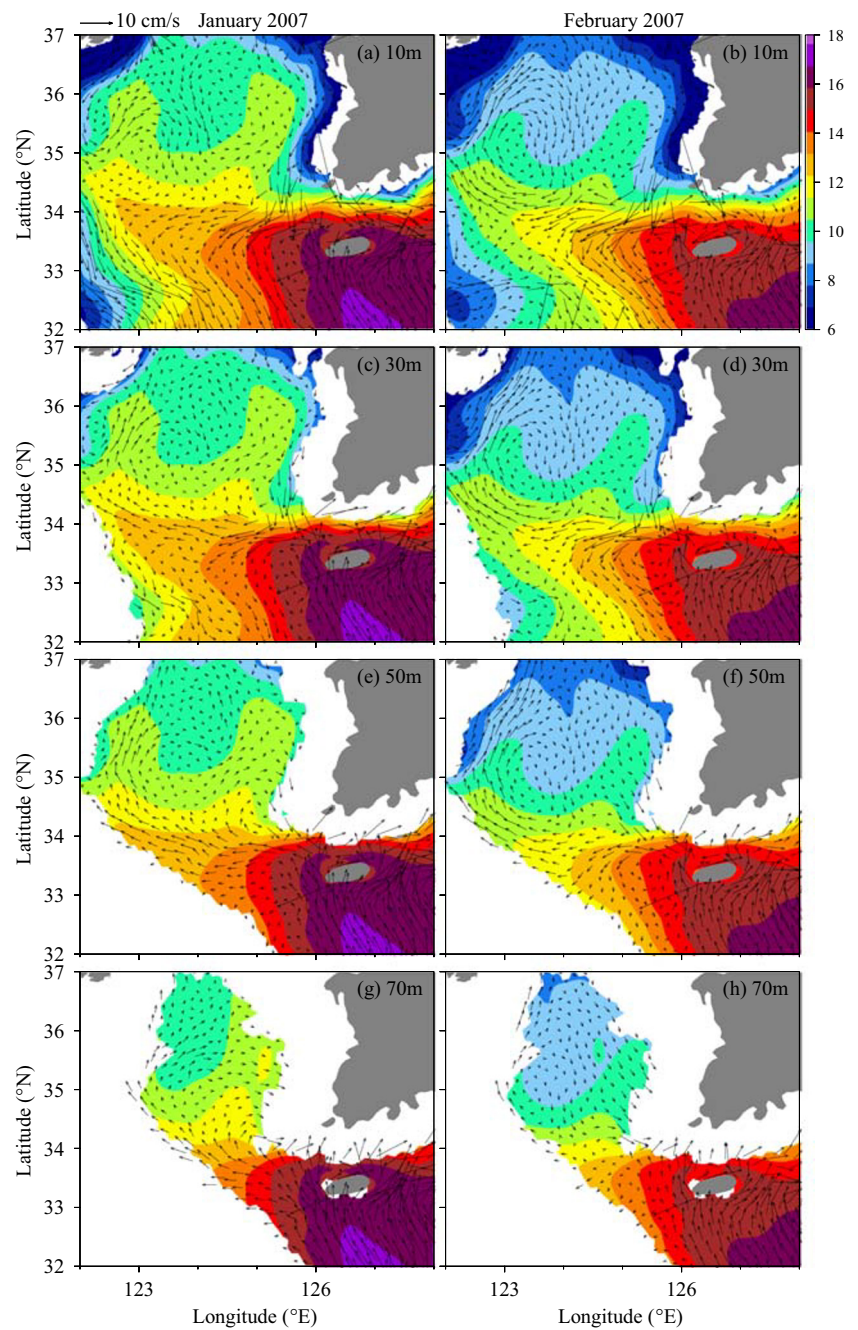
connected directly to the Yellow Sea Warm Current in the western Yellow Sea trough at 50-m depth.

The sea surface height in January and February 2007 was also embedded in the surface (10-m depth) current field (Fig. 10). The region west of Jeju-do was characterized by a low sea surface height and a sea level gradient that increased in the meridional direction. We also showed the sea surface height and surface current derived from Archiving, Validation and Interpretation of Satellite Oceanographic data (AVISO) (c, d) and HYCOM (e, f). It can be noted that the model-simulated sea surface height was higher than that from the AVISO and HYCOM models. In addition, both our model and HYCOM resolved the TC although the intensity of the TC was relatively weaker in the HYCOM model. However, the satellite-derived surface geostrophic currents did not show the westward TC in the region northwest of the Jeju-do.

### 3.3 Vertical structure of the westward TC

The zonal current component ( $u$  velocity), temperature, salinity, and density were sampled along the meridional transect T1 to investigate the vertical structure of the westward TC during

**Fig. 9** The model-simulated monthly mean circulation and temperature at 10-m, 30-m, 50-m, and 70-m depth in January and February 2007

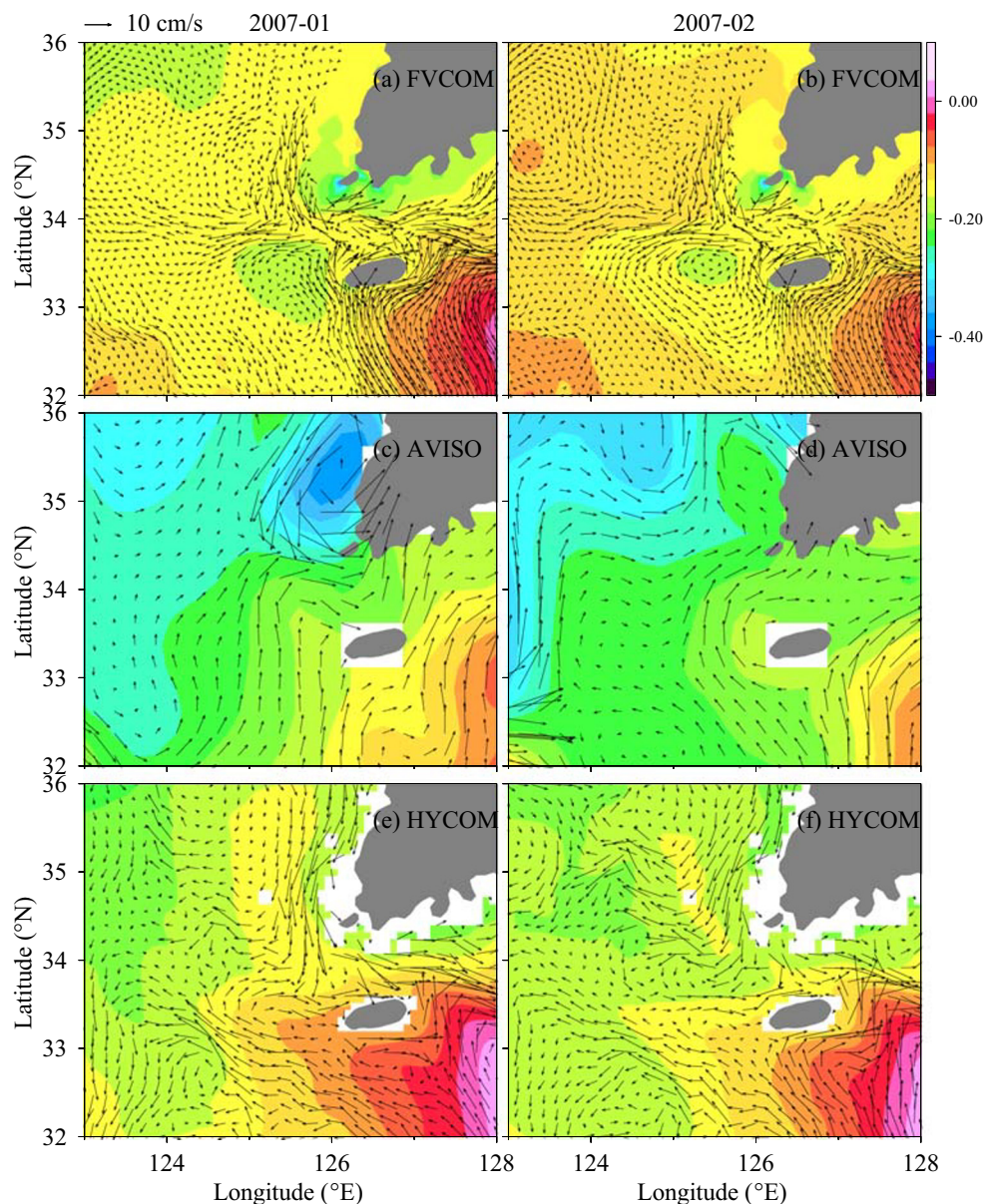


winter 2007 (Fig. 11). The location of transect T1 is marked in Fig. 1. The westward TC extended from the surface to the near-bottom layer in the vertical direction. The magnitude of the westward TC was greatest in the surface layer (velocity > 15 cm/s) and gradually decreased with increasing depth. The magnitude of the westward TC was generally greater than 10 cm/s in layers shallower than 30 m deep. The width of the westward TC in the zonal direction was estimated at about 70 km, and the current axis was located approximately along 33.8° N. There were obvious differences between January and February: the westward TC in February was stronger than the

westward TC in January. Warm saltwater from the south met cold freshwater from the north in the frontal region, which also resulted in a strong density gradient (Fig. 11(g), (h)). Therefore, the thermohaline front was found along transect T1 (Fig. 11(c)–(f)); this corresponded to the maximum magnitude of the westward TC.

We used a zonal transect (T2) across the southern Yellow Sea to sample the current in the southern entrance to the Yellow Sea (Fig. 12). In Fig. 12, the zonal current component ( $u$  velocity) along transect T2 is shown in the upper panel and the meridional current component ( $v$  velocity) is shown in the

**Fig. 10** The monthly mean sea surface height (colors) and surface current (vectors) for FVCOM (a, b), AVISO (c, d), and HYCOM (e, f) in January and February for winter 2007

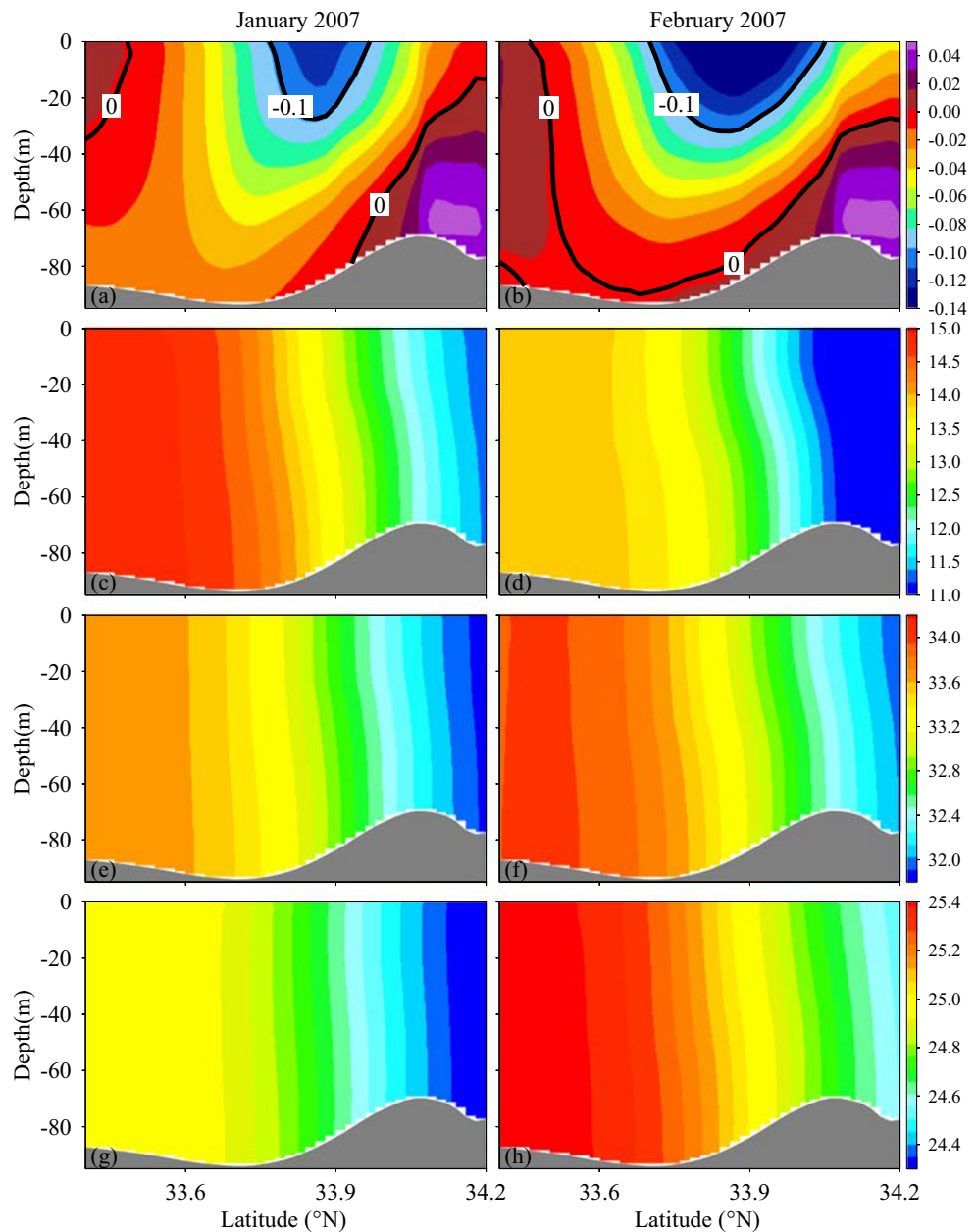


lower panel. Current patterns were similar in January and February. The westward current predominated along the entire transect, with two exceptions: the near-bottom layer in the east and the surface layer in the west. The strong westward TC was mainly limited to the upper layer (shallower than 50 m) and extended from 126° E to 124° E. The westward TC decreased sharply to the west, with the magnitude weakening to 2 cm/s around 123° E (Fig. 12(a), (b)). In the meridional direction, there was a two-layer current pattern along transect T2, with a southward current in the upper layer and a northward current in the lower layer. Northward currents in the eastern transect correspond to the Cheju Warm Current, while the northward Yellow Sea Warm Current was found mainly in the bottom layer of the western transect around 123° E. The southward currents in the upper layer bring cold freshwater to the

northern front, while the northward currents in the lower layer advect warm saltwater to the northern front; these currents normally give rise to the temperature inversions observed in the frontal region (Lie et al. 2015).

We also checked the vertical structure of the TC based on the thermal wind relation as  $f \frac{\partial u}{\partial z} = \frac{1}{\rho_0} \frac{\partial \rho}{\partial y}$ ,  $-f \frac{\partial v}{\partial z} = \frac{g}{\rho_0} \frac{\partial \rho}{\partial x}$ . The vertical shear of horizontal current for the TC was calculated using the thermal wind balance at station N. The horizontal density gradient was adapted from the model results. Figure 13 (a)–(f) show the comparison of vertical shear of TC at station N during the three winter months between the results from thermal wind relation and numerical model. It can be noted that the model-simulated vertical shear of the TC generally agrees with the thermal wind balance during winter

**Fig. 11** The monthly mean current structure (a and b,  $u$  component), temperature (c and d), salinity (e and f), and potential density (g and h) along the meridional transect T1 in the frontal region. The location of transect T1 is shown in Fig. 1. The negative value in (a) and (b) denotes the westward direction



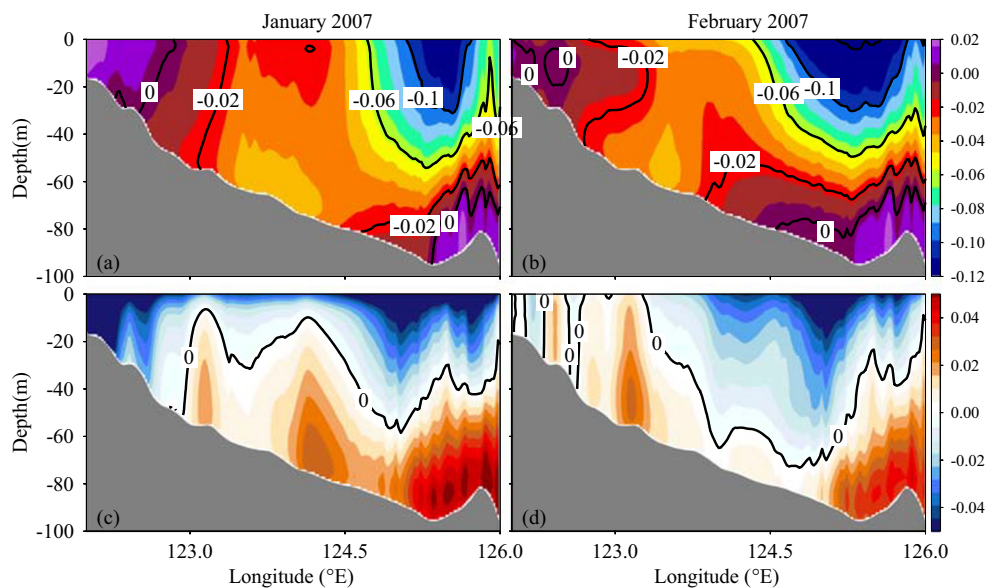
months. Larger discrepancy mainly occurs in the meridional direction ( $dv/dz$ ). If we assume that the bottom current velocity from the thermal wind relation equals that of the model results, we will obtain the vertical distribution of current vectors from the thermal wind relation (Fig. 13(g)–(l)). From the comparison results, we can see that the vertical structure of the TC estimated based on the thermal wind balance is very similar to that from the model simulations during the three winter months. It should be noted that the TC is mainly directed westward with the zonal current component much larger than that of the meridional current component. On the other hand, the density gradient in the zonal direction is more difficult to simulate accurately compared with the density gradient in the

meridional direction. Therefore, the vertical structure for the meridional current component is more difficult to reproduce.

### 3.4 Momentum balance of the westward TC

To examine the dynamics of the westward TC, we performed a momentum balance analysis. The momentum terms in the momentum balance equations were derived based on samples taken from the model results during January and February 2007 at station N (Fig. 1), where the westward TC was dominant. The vertical distributions of currents and momentum terms at station N were determined (Fig. 14). The flow satisfied the conditions of a quasi-geostrophic current. In the

**Fig. 12** The current structures for the zonal current component (a and b) and meridional current component (c and d) along the zonal transect T2. The location for transect T2 is shown in Fig. 1. The negative value in (a) and (b) denotes westward currents. The positive value in (c) and (d) indicates northward currents



meridional momentum equation, the westward current predominated throughout the water column (Fig. 14(a), (d)). In the upper layer of the water column (< 10 m), the westward TC generally exhibited a geostrophic balance, where the meridional barotropic pressure gradient force was largely equivalent to the Coriolis force (Fig. 14(c), (f)). In the lower layer, the baroclinic pressure gradient force became increasingly

important as depth increased; in these layers, the barotropic pressure gradient force was balanced by combined effects of the baroclinic pressure gradient force and the Coriolis force. In addition, the vertical diffusion term and horizontal advection term functioned as second-order terms in the meridional momentum equation. In the zonal momentum equation (Fig. 14(b), (e)), the flow of the TC was dominated by a more

**Fig. 13** Vertical gradient for horizontal current component ( $du/dz$  and  $dv/dz$ ) calculated using thermal wind relation (black line) and model results (red line) during December (a, b), January (c, d), and February (e, f) in winter of 2007. Comparison of current vectors estimated based on thermal wind relation (black arrow) and model results (red arrows) during December, January, and February of 2007 is shown in (g)–(l). The vector at the bottom layer for thermal wind balance was assumed to be equal to the model-simulated bottom current

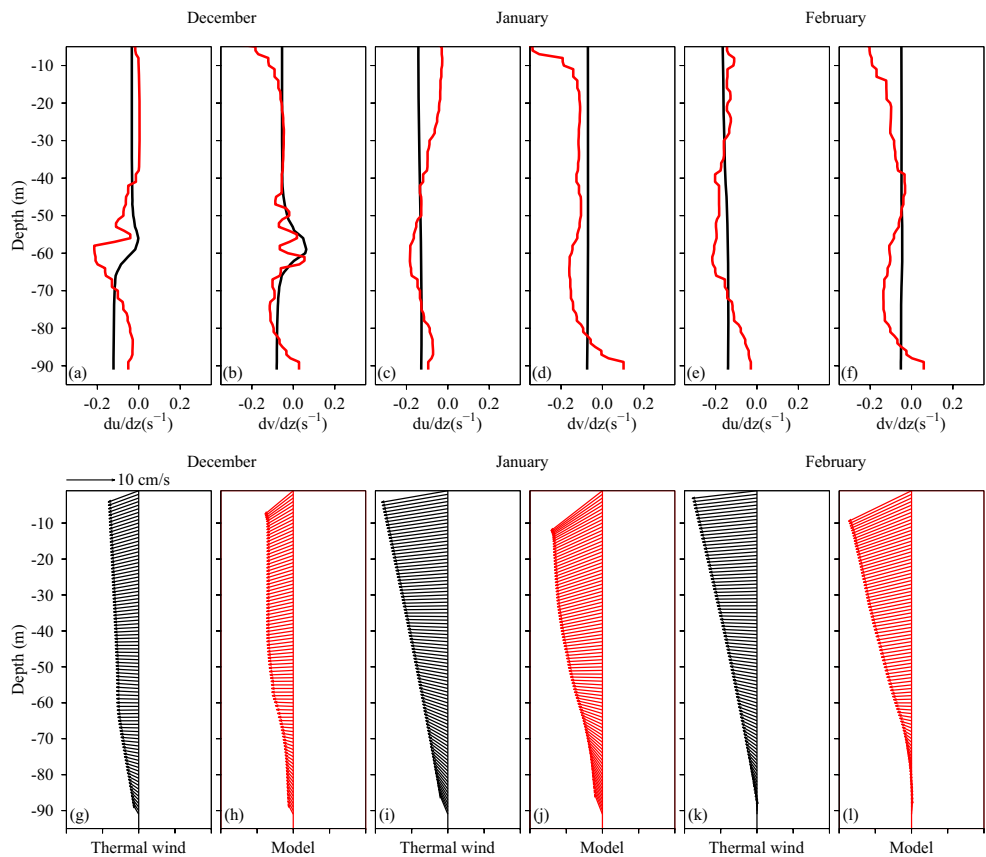
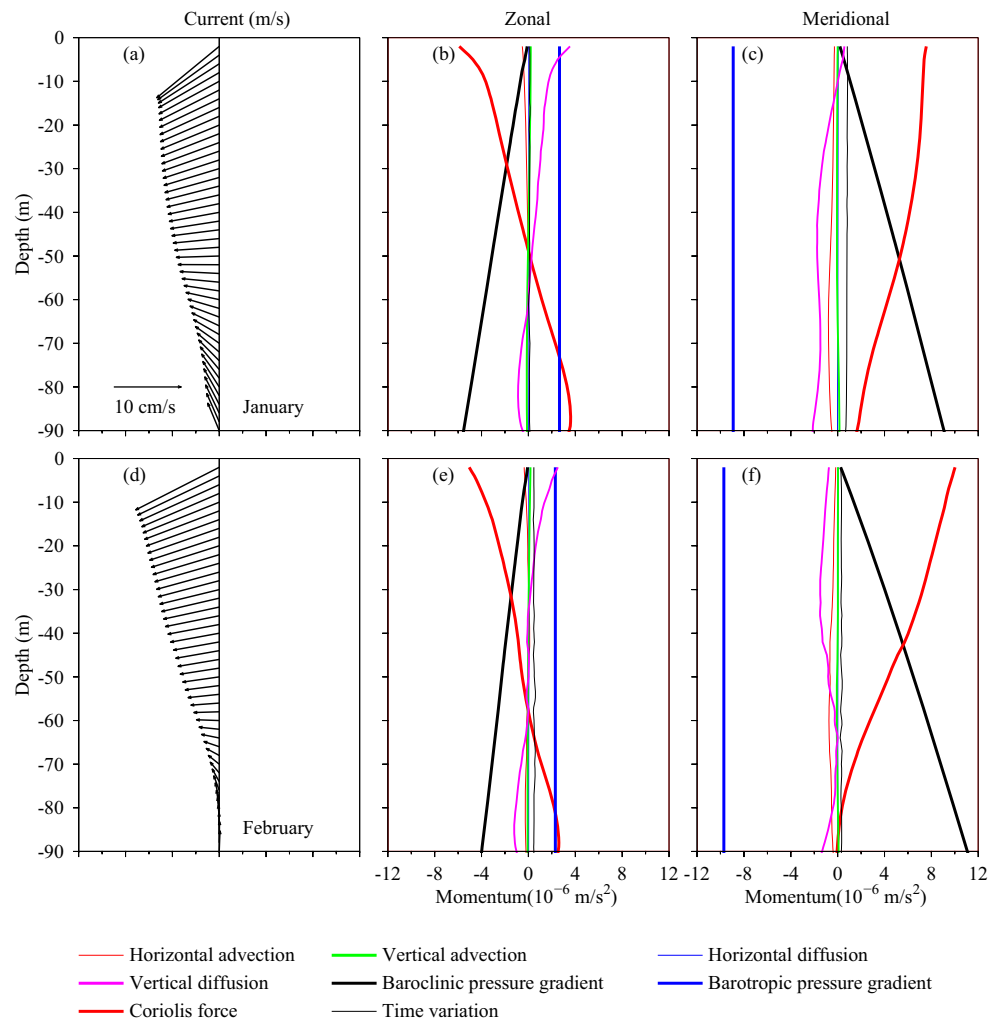


**Fig. 14** The vertical structure of the monthly mean currents (a and d) sampled at station N in the frontal region for January and February 2007. The momentum terms in zonal and meridional directions at the station are also shown in this figure (b, c, e, and f)



complicated process, in which the surface elevation–related barotropic pressure gradient, the baroclinic pressure gradient, the Coriolis force, and the vertical diffusion term were all important and of the same order of magnitude. The zonal Coriolis force changed direction at approximately 50–60 m deep, which indicated a meridional flow reversal in the vertical. The meridional current component featured a southward flow in the upper layer and a northward flow in the lower layer; this pattern was reflected in the current field (Figs. 9 and 12). Similar to the meridional momentum equation, the baroclinic pressure gradient force in the zonal momentum equation also increased with depth. It was worth noting that the monthly average flow was not in a steady state and that the westward TC changed slowly over time.

#### 4 Effects of tide and wind on frontal circulation

The Yellow Sea is characterized by strong tides (Moon et al. 2009). Tide plays an important part in regional mean

circulation in the Yellow Sea because residual currents interact in a nonlinear manner with the topography of the sea floor (An 1977; Choi 1990; Kang et al. 1998; Lee and Beardsley 1999; Kang et al. 2002; Xia et al. 2006; Moon et al. 2009). When investigating frontal circulation and the westward TC in the northern frontal region, Lie et al. (2013) suggested that some wind-driven models might not effectively resolve westward TC and frontal circulation patterns because tidal forcing was neglected. Lie and Cho (2016) also suggested that tidal forcing should be included in numerical models to better reproduce the westward TC in the frontal region. However, the surface wind is one of the main forces driving regional circulation in the Yellow Sea during the winter (Lin et al. 2011; Lie et al. 2013). The winter wind affects the path and the intensity of the Yellow Sea Warm Current (Mask et al. 1998; Wan et al. 2015). The southward coastal currents along both coasts of the Yellow Sea can be strengthened by strong northerly winter winds (Moon et al. 2009). The intermediate northwestward intrusion of the Cheju Warm Current southwest of Jeju-do may be closely associated with northerly wind bursts (Lie et al. 2013). Therefore, to determine the effects of tide and

wind on the frontal circulation and the westward TC, we performed sensitivity experiments, which focused on both tide and wind, as we know that the wind forcing has a great effect in the heat flux calculation based on the bulk formula. Therefore, excluding wind in the model not only affects the advection effect induced by wind-driven currents but also influences the net heat flux. To eliminate the effect of wind

forcing on the heat flux calculation, the heat flux was no longer calculated using the bulk formula in the experiment without wind. Instead, we used the net heat flux and short-wave radiation directly output from the control run to drive the no-wind case. Therefore, the net heat flux used in the no-wind experiment was the same as that used in the control run.

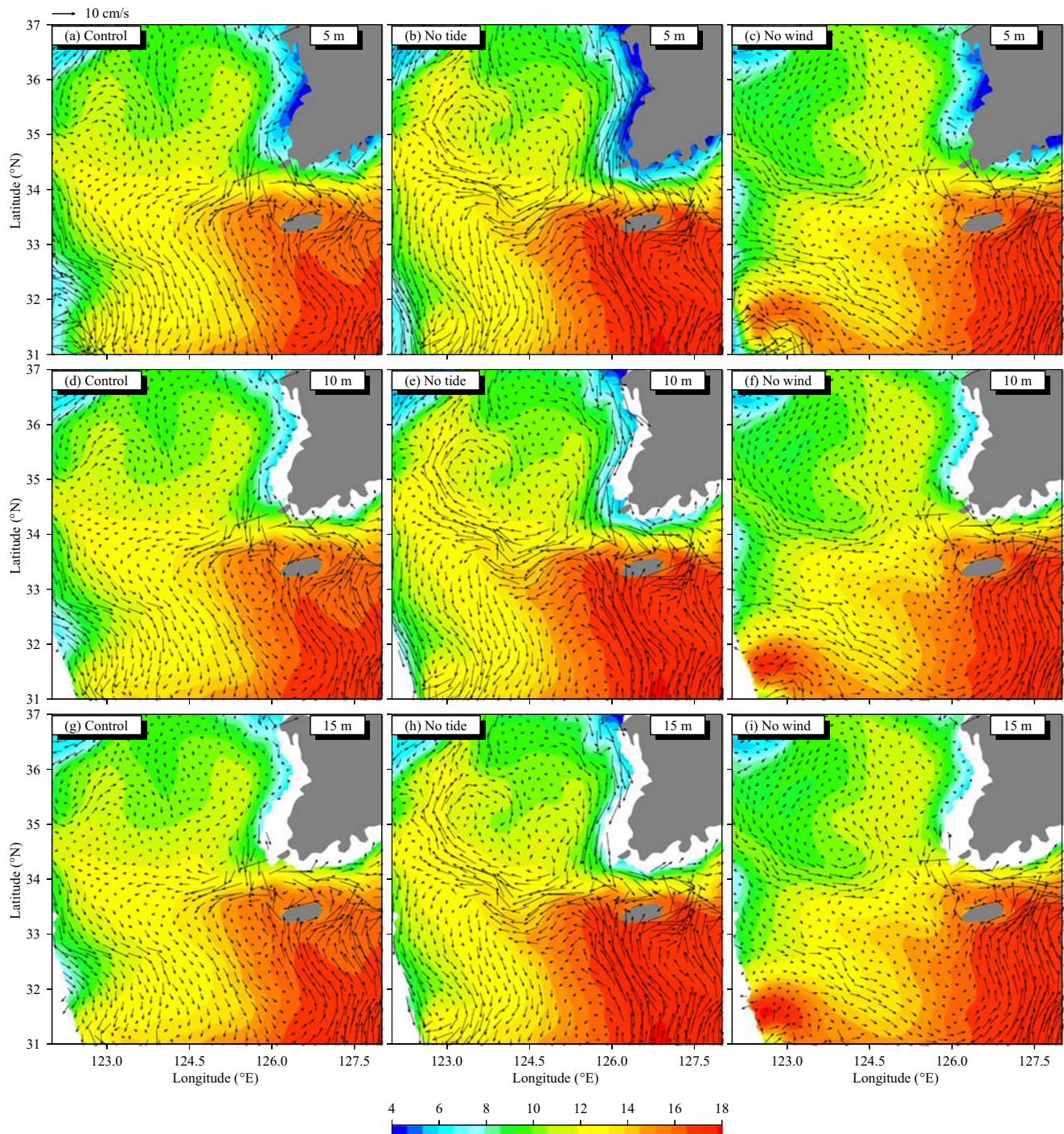


**Fig. 15** Monthly mean current and temperature at 5-m, 10-m, and 15-m depth during January 2007 for control run (a, d, g), no-tide experiment (b, e, h), and no-wind experiment (c, f, i)



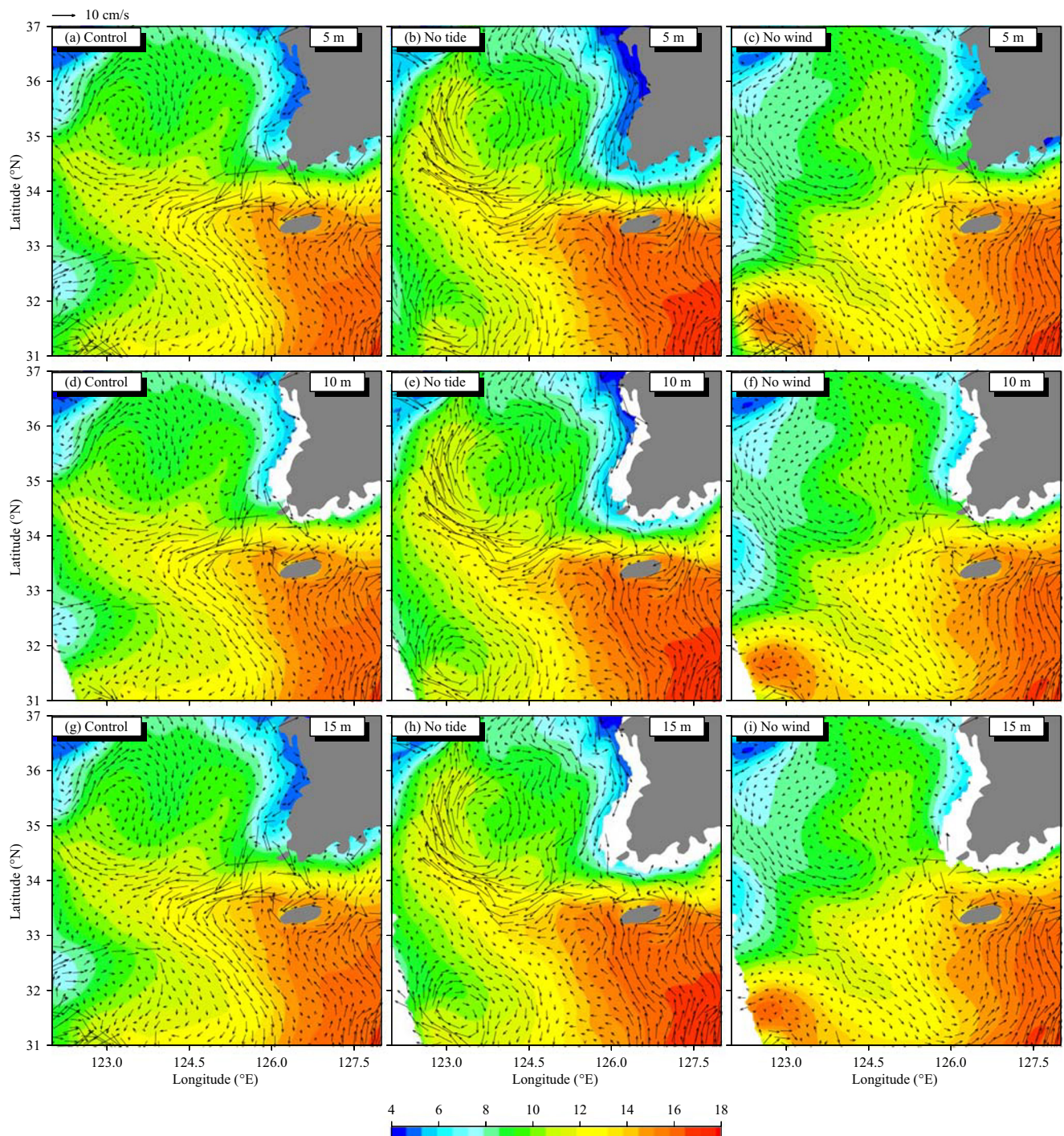


**Fig. 16** Monthly mean current and temperature at 5-m, 10-m, and 15-m depth during February 2007 for control run (a, d, g), no-tide experiment (b, e, h), and no-wind experiment (c, f, i)

We compared control run with experiments excluding wind and with models excluding tide (Figs. 15(b), (e), (h) and 16(b), (e), (h)). In particular, we investigated circulation and temperature at upper layers (5 m, 10 m, and 15 m) in January and February 2007, as the TC mainly located in the upper layers. When tide was excluded from the model (Figs. 15(b), (e), (h) and 16(b), (e), (h)), the model-simulated Yellow Sea Warm

Current along the western Yellow Sea was intensified. In addition, temperature distributions indicated that the warm tongue extended further northwestward into the Yellow Sea interior when tidal forcing was ignored. It is also important to note that both the model-simulated southward Korea Coastal Current and the northward Cheju Warm Current were strengthened in the non-tidal case, which causes the northern

front to be stronger. Notably, the cyclonic circulation around the warm tongue disappeared in the model without tide. The southeastward outflow along the western front was replaced by northwestward current. Currents, temperatures, and salinities differed between the with-tide (control) and without-tide experiments (Fig. S8c, d). The simulations of the without-tide model indicated that temperature and salinity along the western Yellow Sea trough increased 1–2 °C and 1–2 psu (Fig. S8c, d), respectively, due to the intensification of the northwestward Yellow Sea Warm Current. However, the without-tide model simulations also indicated that temperature and salinity north of the northern front decreased, suggesting that more cold freshwater was advected by the intensified southward Korea Coastal Current. It can also be seen that the stronger northward Cheju Warm Current transported more warm saline water to the northern front. Therefore, the density gradient in the meridional direction for the northern frontal zone was strengthened and the northern front became stronger, which led to a stronger TC in the non-tidal case.

The tidal residual current was obtained using a model that included tidal forcing only (Fig. S8e). In this experiment, the southward and southeastward tidal residual currents dominated the western Yellow Sea. In particular, southeastward residual currents off the Changjiang Bank were obvious. The results of our without-tide model experiment were consistent with those of Lie et al. (2009). Interestingly, previous modeling studies suggested that the northwestward upwind flow along the western Yellow Sea entrance was resolved in an ocean model that did not include tide (Jacobs et al. 2000; Ma et al. 2006). It is important to note that the intensity of the tide-rectified residual current is much smaller in magnitude compared with the control run. Therefore, the tidal residual current alone may make minor contribution to the frontal circulation in the southern Yellow Sea. Instead, the mixing and dispersion process associated with tidal forcing may act as a more important factor affecting the structure of density field and thus modify the pattern of the regional circulation in the frontal region. Besides, the friction can be intensified in association with strong tidal current in the shallow coastal region, which tends to decrease the southward Korea Coastal Current (Moon et al. 2009) as also mentioned by one of the reviewers. From the current field and temperature in the non-tidal case (Figs. 15(b), (e), (h) and 16(b), (e), (h)), we can also note that both the southward Korea Coastal Current and the northward Cheju Warm Current were intensified when tidal forcing is removed and the northern front become stronger, which resulted in a stronger TC.

When wind was excluded from the model (Figs. 15(c), (f), (i) and 16(c), (f), (i)), the cyclonic frontal circulation around the warm tongue remained, although with decreased intensity. It is important to note that both the southward Korea Coastal Current and northward Cheju Warm Current were greatly reduced, and the westward TC was also clearly weakened. This

suggested that both the southward Korea Coastal Current and northward Cheju Warm Current contributed to the westward TC, consistent with the results of Lie et al. (2013). The temperature distributions and temperature differences (Fig. S8g) in the model-simulated Yellow Sea showed that the warm water intrusions in the southern Yellow Sea entrance and the western Yellow Sea trough were also reduced when winter wind was ignored. From the current and temperature field in the no-wind run, we can note that both the southward transport of colder water from the Korean coastal region and northward advection of warmer water from the region south of Jeju-do were significantly reduced due to the weakened Korea Coastal Current and Cheju Warm Current. As a result, the temperature and salinity differences simulated by the without-wind model indicated weakened density gradient in the northern frontal region, which induced a much weaker TC. Comparisons among the three experimental models suggested that both tidal forcing and wind forcing were very important for the westward TC along the northern front.

The sea level, temperature, and salinity gradients along transect T1 simulated by the three models were examined (Fig. S8 f, g, and h). In the experiment excluding both tide and wind, the sea level gradient in the meridional direction generally decreased along most of the transect; the sea level gradient decreased further in the models excluding wind only. However, in the without-tide model, the temperature gradient in the meridional direction along the transect increased, while the salinity gradient increased in the transect south of 33.9° N, and decreased in the transect north of 33.9° N. Notably, the temperature and salinity gradients around the northern front were weaker in the model that ignored wind (Fig. S8j, k, black lines). Thus, we concluded that tidal and wind forcing not only influenced the sea surface elevation–related barotropic pressure gradient but also modified the baroclinic gradient; both of these gradients affected the intensity of the frontal circulation and of the westward TC in the frontal zone. When tide was excluded from the model, more warm saltwater was transported from the south, and more cold freshwater moved to the frontal region from the north due to intensification of both the Cheju Warm Current and the Korea Coastal Current. This intensified the northern front in the Yellow Sea entrance and gave stronger westward TC. However, both the northwestward intrusion of the warm, saline Cheju Warm Current and the southward intrusion of the cold, fresh Korea Coastal Current were weakened when wind forcing was ignored, decreasing the density gradients, leading to much weaker TC.

## 5 Relationship between the westward TC and the Yellow Sea Warm Current

In winter, the Yellow Sea Warm Current, which may be closely related to the warm, saline tongue in the frontal region (Lie

et al. 2009; Lie et al. 2013), acts as an important link between the East China Sea and the Yellow Sea: the Yellow Sea Warm Current advects warm saltwater from the frontal zone to the Yellow Sea interior (Lie et al. 2009; Lin et al. 2011). Lie et al. (2009) argued that the Yellow Sea Warm Current was associated with the occasional collapse of the thermohaline front in response to winter storm bursts. Observed trajectories of floats deployed in the frontal region also indicate that the westward TC transports water along the northern front westward across the Yellow Sea trough (Lie et al. 2013). This frontal water then intrudes northwestward into the Yellow Sea Warm Current. Interestingly, our model results (Sect. 3.1) suggested that part of the water from the westward TC continued to move northwestward and joined the Yellow Sea Warm Current in the western Yellow Sea trough (Fig. 9). This finding raised two questions. First, is there a close link between the westward TC and the Yellow Sea Warm Current in the Yellow Sea? Second, are the properties of the water in the Yellow Sea Warm Current influenced by the frontal circulation in the southern Yellow Sea entrance? We aimed to answer these questions using our model.

### 5.1 Volume transport of the westward TC and the Yellow Sea Warm Current

Based on the path of the westward TC and the northwestward Yellow Sea Warm Current along the western Yellow Sea trough, we focused on two transects: the meridional transect T1 and the zonal transect T3, stretching from the 50- to 70-m isobaths along 35° N; the locations of both transects are shown in Fig. 1. We calculated the time series of volume transport through each transect based on our model results (Fig. 17). The positive transport values indicated westward transport induced by the TC and northward transport related to the Yellow Sea Warm Current. It is worth noting that the two volume-transport time series, describing the westward TC and Yellow Sea Warm Current, were closely related. The variations in Yellow Sea Warm Current transport were closely associated with those in TC transport. The correlation coefficient between the two volume-transport time series was estimated at 0.55 (> 95% confidence). When the westward

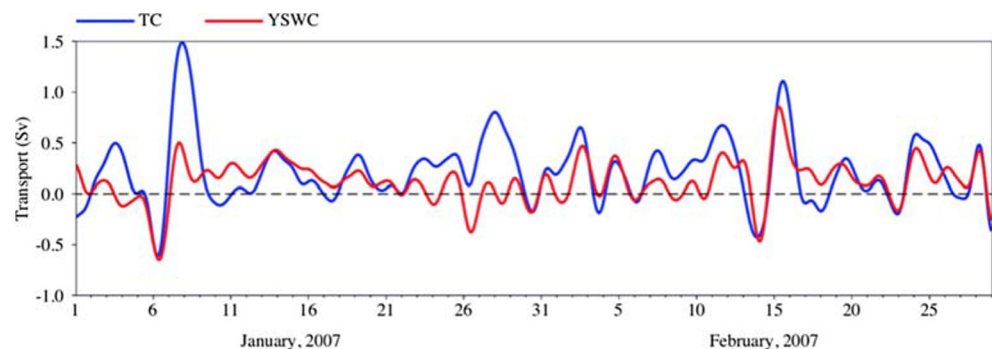
transport of the TC increased, the northward transport of the Yellow Sea Warm Current also increased, and vice versa. This correspondence was especially obvious during the two storm events (January 5–10 and February 12–17). The transport values for both the TC and the Yellow Sea Warm Current peaked during these storm events, and the significant fluctuations in volume transport through the two transects were congruent. This might reflect the close association between the westward TC and the Yellow Sea Warm Current.

### 5.2 Lagrangian particle tracking experiments

To further examine the relationship between frontal circulation and the Yellow Sea Warm Current during the winter, we performed Lagrangian particle tracking experiments (Fig. 18). Particles (black dots) were first released at 10-m, 30-m, and 50-m depth in two regions (west of Korea and south of Jeju-do) to track the movements of cold freshwater from the Korea Coastal Current and warm saltwater from the Cheju Warm Current, respectively (Fig. 18(a)–(c)). The particles were released on December 20, 2006, and tracked for more than 4 months.

For the particles released at 10-m depth (Fig. 18(a), blue lines), most of particles from the Korea Coastal Current moved southward to the northern front and continued to progress westward along the northern front without crossing the front. The particles then moved cyclonically around the western tip of the front and continued to shift southeastward, without escaping from the warm tongue. The trajectories of these particles were consistent with the modeled circulation patterns (Fig. 9(a), (b)). The particles released south of Jeju-do moved northward and bifurcated when encountering Jeju-do, with some of the particles turning anti-cyclonically around Jeju-do. Notably, no surface particles were observed to join the Yellow Sea Warm Current. However, one particle moved westward as far as 123° E before it turned southeastward to join the Southeastward Outflow. At 30-m depth (Fig. 18(b)), the particles from the Korea Coastal Current and those from the Cheju Warm Current met in the frontal region west of Jeju-do. Some particles originating from the Korea Coastal Current were transported northwestward into the western Yellow Sea

**Fig. 17** The volume transport across transects T1 and T3 for the westward TC (blue) and YSWC (red)



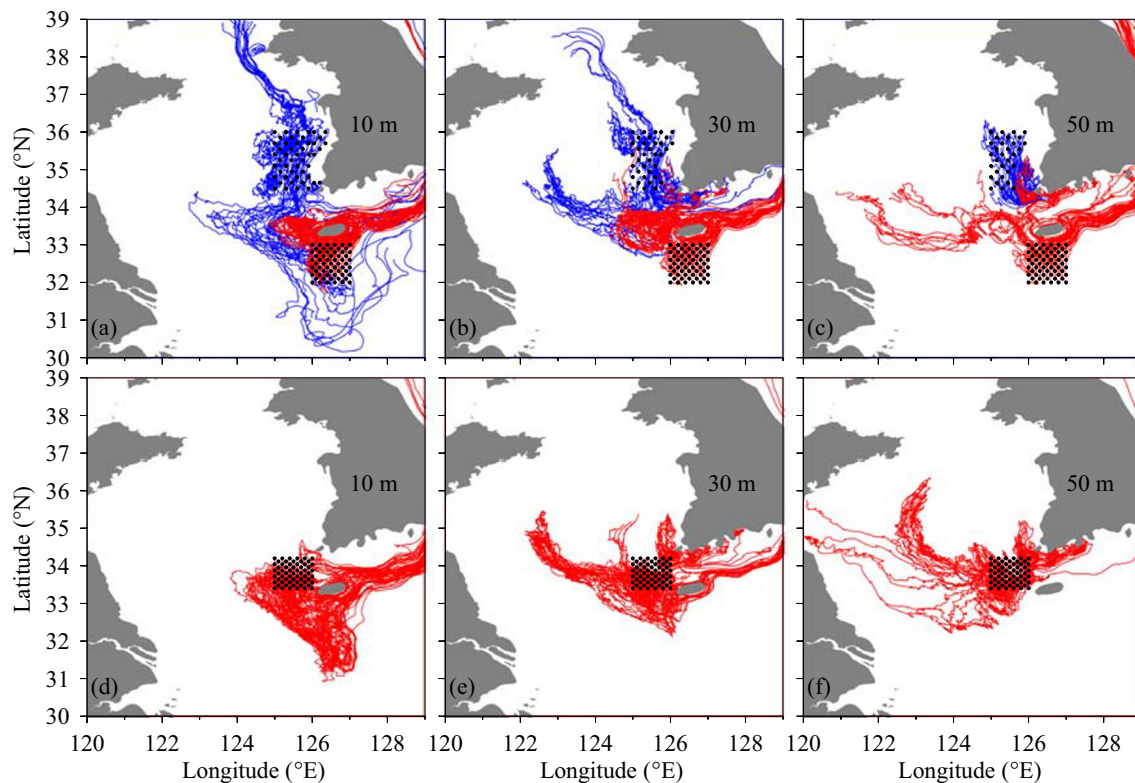


**Fig. 18** Trajectories of the particles released west of Korean (blue) and south of Jeju-do (red) at 10-m (a), 30-m (b), and 50-m (c) depth. The trajectories of the particles released at the frontal region are shown in (d)–(f). The black dots denote the initial locations of the particles

and joined the Yellow Sea Warm Current. At 50-m depth (Fig. 18(c)), some of the particles from the Cheju Warm Current moved to the frontal zone and then continued to progress northward to the western Yellow Sea.

The westward TC is closely related to advection of cold freshwater from the southward Korea Coastal Current and the warm saltwater from the Cheju Warm Current (Lie et al. 2015; Lie and Cho 2016). Based on our experimental models, the properties of the surface (10 m) water in the frontal region were more strongly influenced by the cold freshwater from the southward Korea Coastal Current. However, the sub-surface water (30 m) in the frontal region mixed with both the cold freshwater from southward Korea Coastal Current and warm saltwater from the northward Cheju Warm Current. In the deeper layer (50 m), the characteristics of the water in the frontal region were mainly determined by the northward intrusion of the Cheju Warm Current.

Another experiment was performed with particles released in the frontal region, to track the movement of the frontal water. At 10-m depth (Fig. 18(d)), most of the particles moved cyclonically around the warm tongue and were transported southeastward to join the Cheju Warm Current. Then, the particles moved northward, along with the Cheju Warm Current, and entered the Tsushima Strait. At 30-m depth (Fig. 18(e)), some particles in the frontal region moved northward into the Yellow Sea Warm Current and then were

transported northward along the western trough. Importantly, the trajectories of these particles were consistent with the path of the Yellow Sea Warm Current. However, some particles appeared to become trapped in the frontal region. At 50-m depth (Fig. 18(f)), the particles released in the frontal region mainly moved northward, which indicated the trajectory of the Yellow Sea Warm Current.

It can thus be concluded that the water in the frontal region typically mixes with both the cold freshwater from the north and the warm saltwater from the south. Both the southward Korea Coastal Current and northward intrusion of the Cheju Warm Current contributed to the water features in the frontal zone. Based on the particle trajectories in the experimental models, some of the water in the frontal region, particularly from the sub-surface and bottom layers, was transported northward into the Yellow Sea interior by the Yellow Sea Warm Current. Therefore, the properties of the water in the frontal region partially determined the character of the Yellow Sea Warm Current. In the northern frontal region during the winter, the westward TC transported water in the eastern Yellow Sea westward along the front, across the deep trough in the southern Yellow Sea entrance. Lie et al. (2013) proposed that the westward TC was a continuation of southward Korea Coastal Current. The results of our Lagrangian experiments were consistent with this theory. However, we

also found that the westward TC connected the frontal zone to the Yellow Sea Warm Current.

## 6 Conclusions

Here, we characterized the spatial distributions and the detailed structures of the westward TC and the frontal circulation in the southern Yellow Sea entrance during the winter using a three-dimensional ocean model. Model-data comparisons indicated that our model accurately modeled the frontal circulation and the westward TC. We thus used this model in subsequent experiments.

The westward TC and the cyclonic frontal circulation were characterized by surface intensity, which decreased gradually with increasing depth. The westward TC spanned 100–200 km in the zonal direction. The width of the westward TC in the meridional direction was about 50–70 km, with the major axis essentially following 33.8° N. Sensitivity experiments using tide and wind indicated that these factors had a positive effect on the frontal circulation as well as the westward TC. Specifically, tide and wind established a barotropic pressure gradient associated with the sea level and modulated the density gradient. These gradients affected the structure and intensity of the westward TC in the frontal region.

The Yellow Sea Warm Current volume transport was highly correlated with the TC transport, suggesting that the westward TC and the Yellow Sea Warm Current were closely related during the winter. Our Lagrangian particle tracking experiments indicated that the properties of the surface water in the frontal region are more influenced by the cold freshwater from the southward Korea Coastal Current. The subsurface water in the frontal region was mixed with both the cold, freshwater from north and warm saltwater from the northward Cheju Warm Current. In the deep layer, the characteristics of the water in the frontal region were mainly determined by the northwestward intrusion of the Cheju Warm Current. To some extent, the properties of the water in the Yellow Sea Warm Current were related to those of the water in the frontal region. The westward TC not only linked the cold, fresh Korea Coastal Current with the frontal zone but also connected the frontal region west of Jeju-do with the Yellow Sea Warm Current along the western Yellow Sea trough. The TC usually flowed westward along the northern front. According to Lie et al. (2013), the TC separates into two branches with one flowing northwestward into the Yellow Sea interior and the other turning cyclonic around the tip of the front and flowing southeastward. As the TC is usually mixed with water both from the cold/fresh Korea Coastal Current and warm/saline Cheju Warm Current, its intensity and variability may significantly influence the distribution of hydrodynamics and nutrient in this region. The TC is able to transport mixed water in the frontal region westward and is often connected

with the Yellow Sea Warm Current. Therefore, the westward TC may play a very important role in the regional circulation and also ecosystem in the frontal region.

Although ocean models may help us to understand the characteristics and dynamic mechanisms of the frontal circulation in the southern Yellow Sea entrance, additional observations, especially direct long-time current measurements, are still needed in this region in the near future. Such observations are vital for accurate depictions of the multi-scale features and interannual variability of the frontal circulation. Based on these observations and numerical model results, the important effect of the TC on the regional circulation and ecosystem in this region should be further investigated in future study.

**Acknowledgments** All model simulations were performed in the Data and Simulation Center of Physical Oceanography Laboratory, Ocean University of China. We are grateful to the University of Hawaii Sea Level Center, Hybrid Coordinate Ocean Model, National Center for Environmental Prediction (NCEP), Korean Oceanographic Data Center, OSU Tidal Data Inversion, and Bureau of Hydrology, Ministry of Water Resources of P. R. China, for providing valuable data. We thank LetPub ([www.letpub.com](http://www.letpub.com)) for its linguistic assistance during the preparation of this manuscript. We also thank the editor and the three reviewers for carefully reviewing the manuscript and providing valuable suggestions.

**Funding information** This work was funded by the National Natural Science Foundation of China (grant numbers 41430963, 41876006, 41676004, 41476047), National Fund Committee-Shandong joint fund (No. U1706215), and National Program on Global Change and Air-Sea Interaction (No. GASI-GEOGE-03).

## References

- An HS (1977) A numerical experiment of the M2 tide in the Yellow Sea. *J Oceanogr Soc Jpn* 33:103–110. <https://doi.org/10.1007/BF02110016>
- Asaoka O, Moriyasu S (1966) On the circulation in the East China Sea and the Yellow Sea in winter (preliminary report). *Oceanogr Mag* 18:73–81
- Bao X, Su J, Guo X, Wu D (2004) Simulation of seasonal variation of thermo-structure and circulation in the Bohai and Yellow Seas. *J Ocean Univ China* 34(4):513–522 (In Chinese with English abstract)
- Beardsley, R. C., and Rosenfeld, L. K., 1983. Introduction to the CODE-1 moored array and large-scale data report, in CODE-1: moored array and large-scale data report, edited by L. K. Rosenfeld, Woods Hole Oceanogr. Inst. Tech. Rep. WHOI-83-23, CODE tech. Rep. 21, pp. 1216, Woods Hole Inst. Of Oceanogr., Woods Hole, Mass
- Bleck R (2002) An oceanic general circulation model framed in hybrid isopycnic-Cartesian coordinates. *Ocean Model* 4(1):55–88
- Chassignet EP, Hurlburt HE, Smedstad OM, Halliwell GR, Hogan PJ, Wallcraft AJ, Bleck R (2007) The HYCOM (hybrid coordinate ocean model) data assimilative system. *J Mar Syst* 65(1):60–83
- Chen C, Liu H, Beardsley RC (2003) An unstructured, finite-volume, three-dimensional, primitive equation ocean model: application to coastal ocean and estuaries. *J Atmos Ocean Technol* 20:159–186. <https://doi.org/10.1175/1520-0426>
- Chen CS, Huang HS, Beardsley RC, Liu HD, Xu QC, Cowles G (2007) A finite-volume numerical approach for coastal ocean circulation

- studies: comparisons with finite difference models. *J Geophys Res* 112(C03018):1–34. <https://doi.org/10.1029/2006JC003485>
- Chen C, Xue P, Ding P, Beardsley RC, Xu Q, Mao X et al (2008) Physical mechanisms for the offshore detachment of the Chanjiang diluted water in the East China Sea. *J Geophys Res* 113:C02002. <https://doi.org/10.1029/2006JC003994>
- Choi BH (1990) Development of fine-grid numerical tidal models of the Yellow Sea and the East China Sea. *J Korean Soc Coastal Ocean Eng* 4:233–244
- Ding Y, Yu HM, Bao XW, Kuang L, Wang CX, Wang WJ (2011) Numerical study of the barotropic responses to a rapidly moving typhoon in the East China Sea. *Ocean Dyn* 61:1237–1259. <https://doi.org/10.1007/s10236-011-0436-1>
- Ding Y, Bao X, Yao Z, Song D, Song J, Gao J, Li J (2018) Effect of coastal-trapped waves on the synoptic variations of the Yellow Sea Warm Current during winter. *Cont Shelf Res* 167:14–31
- Egbert G, Erofeeva S (2002) Efficient inverse modeling of barotropic ocean tides. *J Atmos Ocean Technol* 19:22,475–22,502
- Fairall CW, Bradley EF, Rogers DP, Edson JB, Young GS (1996) Bulk parameterization of air-sea fluxes for Tropical Ocean-Global Atmosphere Coupled–Ocean Atmosphere Response Experiment. *J Geophys Res* 101(C2):3747–3764. <https://doi.org/10.1029/95JC03205>
- Ge J, Shen F, Guo W, Chen C, Ding P (2015) Estimation of critical shear stress for erosion in the Changjiang Estuary: a synergy research of observation, GOCI sensing and modeling. *J Geophys Res* 120: 8439–8465. <https://doi.org/10.1002/2015JC010992>
- Guan B (1962) Some problems concerning the study of the current structure of the nearshore area of the China sea. *Ocean Lim Sin* 4(3–4): 121–141 (in Chinese with English abstract)
- Guan BX (1994) Patterns and structures of the currents in Bohai, Huanghai and East China Seas. In: Zhou D, Liang YB, Zeng C-K (eds) *Oceanology of China seas, vol 1*. Kluwer Academic Publishers, Dordrecht, pp 17–26
- Hao J, Chen Y, Wang F (2010) Temperature inversion in China seas. *J Geophys Res* 115:C12025. <https://doi.org/10.1029/2010JC006297>
- Huang D, Zhang T, Zhou F (2010) Sea-surface temperature fronts in the Yellow and East China Seas from TRMM microwave imager data. *Deep Sea Res Part II* 57:1017–1024
- Ichikawa H, Beardsley RC (2002) The current system in the Yellow and East China Seas. *J Oceanogr* 58:77–92
- Isobe A (2008) Recent advances in ocean-circulation research on the Yellow Sea and East China Sea shelves. *J Oceanogr* 64(4):569–584. <https://doi.org/10.1007/s10872-008-0048-7>
- Jin J, Liu SM, Ren JL, Liu CG, Zhang J, Zhang ZL, Huang DJ (2013) Nutrient dynamics and coupling with phytoplankton species composition during the spring blooms in the Yellow Sea. *Deep Sea Res II Top Stud Oceanogr* 97:16–32. <https://doi.org/10.1016/j.dsr2.2013.05.002>
- Jacobs GA, Hur HB, Riedlinger SK (2000) Yellow and East China Seas response to winds and currents. *J Geophys Res* 105:21,947–21,968
- Kang SK, Lee SR, Lie HJ (1998) Fine grid tidal modeling of the Yellow and East China seas. *Cont Shelf Res* 18:739–772. [https://doi.org/10.1016/S0278-4343\(98\)00014-4](https://doi.org/10.1016/S0278-4343(98)00014-4)
- Kang SK, Foreman MGG, Lie HJ, Lee JH, Cherniawsky J, Yum KD (2002) Two-layer tidal modeling of the Yellow and East China seas with application to seasonal variability of the M2 tide. *J Geophys Res* 107(C3):3020. <https://doi.org/10.1029/2001JC000838>
- Kim HJ, Yoon HJ, Yang SK (1982) Inversion phenomena of temperature in the Yellow Sea. *Bull Korean Fish Tech Soc* 18(2):91–96
- Lee SH, Beardsley RC (1999) Influence of stratification on residual tidal currents in the Yellow Sea. *J Geophys Res* 104:15,679–15,701
- Lie HJ (1984) A note on water masses and general circulation in the Yellow Sea (Hwanghae). *J Oceanol Soc Korean* 19:187–194
- Lie HJ (1985) Wintertime temperature-salinity characteristics in the southeastern Hwanghae (Yellow Sea). *J Oceanogr Soc Jpn* 41: 291–298
- Lie HJ, Cho CH, Lee JH, Lee S, Tang Y, Zou E (2001) Does the Yellow Sea Warm Current really exist as a persistent mean flow? *J Geophys Res* 106:22,199–22,210
- Lie HJ, Cho CH, Lee S (2009) Tongue-shaped frontal structure and warm water intrusion in the southern Yellow Sea in winter. *J Geophys Res* 114:C01003. <https://doi.org/10.1029/2007JC004683>
- Lie HJ, Cho CH, Lee S (2013) Frontal circulation and westward transversal current at the Yellow Sea entrance in winter. *J Geophys Res Oceans* 118:3851–3870. <https://doi.org/10.1002/jgrc.20280>
- Lie HJ, Cho CH, Jung KT (2015) Occurrence of large temperature inversion in the thermohaline frontal zone at the Yellow Sea entrance in winter and its relation to advection. *J Geophys Res Oceans* 120: 417–435. <https://doi.org/10.1002/2014JC010653>
- Lin X, Yang J, Guo J, Zhang Z, Yin Y, Song X, Zhang X (2011) An asymmetric upwind flow, Yellow Sea Warm Current: 1. New observations in the western Yellow Sea. *J Geophys Res* 116:C04026. <https://doi.org/10.1029/2010JC006513>
- Lin X, Yang J (2011) An asymmetric upwind flow, Yellow Sea Warm Current: 2. Arrested topographic waves in response to the north-westerly wind. *J Geophys Res* 116:C04027. <https://doi.org/10.1029/2010JC006514>
- Liu X, Chiang KP, Liu SM, Wei H, Zhao Y, Huang BQ (2015) Influence of the Yellow Sea warm current on phytoplankton community in the central Yellow Sea. *Deep Sea Res Part I* 106:17–29
- Lie HJ, Cho CH (2016) Seasonal circulation patterns of the Yellow and East China Seas derived from satellite-tracked drifter trajectories and hydrographic observations. *Prog Oceanogr* 146:121–141
- Ma J, Qiao F, Xia C, Kim CS (2006) Effects of the Yellow Sea Warm Current on the winter temperature distribution in a numerical model. *J Geophys Res* 111:C11S04. <https://doi.org/10.1029/2005JC003171>
- Mask AC, O'Brien JJ, Preller R (1998) Wind-driven effects on the Yellow Sea Warm Current. *J Geophys Res* 103:30,713–30,729. <https://doi.org/10.1029/1998JC900007>
- Moon JH, Hirose N, Yoon JH (2009) Comparison of wind and tidal contributions to seasonal circulation of the Yellow Sea. *J Geophys Res* 114:C08016. <https://doi.org/10.1029/2009JC005314>
- Nakao T (1977) *Oceanic variability in relation to fisheries in the East China Sea and the Yellow Sea*. Tokai University (Special No), Journal of Marine Science and Technology, pp 199–367
- Oh KH, Lee S, Lie HJ, Jung KT, Qiao F (2015) Study on the current structure of the thermohaline front in the southeastern entrance of the Yellow Sea during winter. *Acta Oceanol Sin* 34(12):29–36. <https://doi.org/10.1007/s13131-015-0763-z>
- Pang IC, Moon JH, Lee JH, Hong JS, Pang SJ (2017) Modeling temperature inversion in southeastern Yellow Sea during winter 2016. *J Geophys Res Oceans*:122. <https://doi.org/10.1002/2017JC012718>
- Park S, Chu PC (2006) Thermal and haline fronts in the Yellow/East China Seas: surface and subsurface seasonality comparison. *J Oceanogr* 62:617–638
- Su J, Wu H, Zhang Y, Liu Q, Bai S (2005) A coupled ice-ocean model for the Bohai Sea: part II. Case study. *Acta Oceanol Sin* 24:54–67
- US Naval Oceanographic Office and the US Naval Ocean Research and Development Activity (1983) *DBDB5 (Digital Bathymetric Data Base-5 minute grid)*. US N.O.O, Bay St. Louis, p 329
- Wan K, Bao X, Wang Y, Wan X, Li H, Liu K (2015) Barotropic current fluctuations coupled with sea level drawdown in Yellow and Bohai Seas. *Chin J Oceanol Limnol* 33(1):272–281. <https://doi.org/10.1007/s00343-015-4056-3>
- Wang F, Liu C, Meng Q (2012) Effect of the Yellow Sea warm current fronts on the westward shift of the Yellow Sea warm tongue in winter. *Cont Shelf Res* 45:98–107

- Wei H, Shi J, Lu YY, Peng YA (2010) Interannual and long-term hydrographic changes in the Yellow Sea during 1977-1998. *Deep Sea Res II Top Stud Oceanogr* 57(11–12):1025–1034. <https://doi.org/10.1016/j.dsr2.2010.02.004>
- Xia C, Qiao F, Yang Y, Ma J, Yuan Y (2006) Three-dimensional structure of the summertime circulation in the Yellow Sea from a wave-tide-circulation coupled model. *J Geophys Res* 111:C11S03. <https://doi.org/10.1029/2005JC003218>
- Xuan J, Huang D, Pohlmann T, Su J, Mayer B, Ding R, Zhou F (2017) Synoptic fluctuations of the Taiwan Warm Current in winter on the East China Sea shelf. *Ocean Sci* 13:105–122
- Xue P, Chen C, Ding P, Beardsley RC, Lin H, Ge J, Kong Y (2009) Saltwater intrusion into the Changjiang River: a model-guided mechanism study. *J Geophys Res* 114:C02006. <https://doi.org/10.1029/2008JC004831>
- Yuan D, Zhu J, Li C, Hu D (2008) Cross-shelf circulation in the Yellow and East China Seas indicated by MODIS satellite observations. *J Mar Syst* 70:134–149
- Yu F, Zhang Z, Diao X, Guo J (2010) The observation evidence of the Yellow Sea Warm Current. *Chin J Oceanol Limnol* 28:677–683. <https://doi.org/10.1007/s00343-010-0006-2>